Akinribide, Ojo Jeremiah; Mekgwe, Gadifele Nicolene; Akinwamide, Samuel Olukayode; Gamaoun, Fehmi; Abeykoon, Chamil; Johnson, Oluwagbenga T.; Olubambi, Peter Apata

A review on optical properties and application of transparent ceramics

Published in:
Journal of Materials Research and Technology

DOI:
10.1016/j.jmrt.2022.09.027

Published: 01/01/2022

Document Version
Publisher's PDF, also known as Version of record

Please cite the original version:
Akinribide, O. J., Mekgwe, G. N., Akinwamide, S. O., Gamaoun, F., Abeykoon, C., Johnson, O. T., & Olubambi, P. A. (2022). A review on optical properties and application of transparent ceramics. *Journal of Materials Research and Technology*, *21*, 712-738. https://doi.org/10.1016/j.jmrt.2022.09.027

JOURNAL OF MATERIALS RESEARCH AND TECHNOLOGY 2022;21:712–738

Available online at www.sciencedirect.com

jmr&t
Journal of Materials Research and Technology

journal homepage: www.elsevier.com/locate/jmrt

Review Article

A review on optical properties and application of transparent ceramics

Ojo Jeremiah Akinribide [a,*], Gadifele Nicolene Mekgwe [a],
Samuel Olukayode Akinwamide [c], Fehmi Gamaoun [b], Chamil Abeykoon [d],
Oluwagbenga T. Johnson [e], Peter Apata Olubambi [a]

[a] Center for Nanomechanics and Tribocorrosion, School of Mining, Metallurgy and Chemical Engineering, University of Johannesburg, South Africa
[b] Mechanical Engineering Department, College of Engineering, King Khalid University, Abha, 61421, Saudi Arabia
[c] Department of Mechanical Engineering, Aalto University, Espoo, Finland
[d] Northwest Composites Centre and Aerospace Research Institute, Department of Materials, Faculty of Science and Engineering, The University of Manchester, Oxford Road, M13 9PL, Manchester, UK
[e] Department of Mining and Metallurgical Engineering, University of Namibia, Ongwediva, Namibia

ARTICLE INFO

Article history:
Received 27 May 2022
Accepted 7 September 2022
Available online 20 September 2022

Keywords:
Transparent YSZ
Sintering technologies
Optical properties
Refractive index
Optical transparency

ABSTRACT

Advanced expertise and technologies have been devoted to producing high functional materials with a polycrystalline nature, which is transparent to visible light for various manufacturing applications. Materials with a good lattice structure can also be adopted in the manufacturing of transparent ceramics. Observations from the literature showed that oxide-based transparent ceramics had been successfully utilized, owing to their remarkable mechanical properties, chemical stability, and a wide range of flexible synthesis routes. Translucent zirconia (ZrO2) ceramics have drawn enormous attention from researchers in different fields due to their outstanding properties such as oxygen (O2) conductivity, mechanical behavior, functional properties, high level of toughness, and thermal conductivity. The Cubic and tetragonal crystal structure of zirconia can be applied for stabilizing Yttria (Y_2O_3) to enhance its optical performance and mechanical strength. Due to high chemical stability and high refractive index within the range of 2.2, transparent yttria-stabilized zirconia ceramic has been found useable in varying applications, including electromagnetic radiation, and camera lenses. The purity of starting materials and sintering techniques has been considered the proper production process for obtaining fully dense ceramics with less than 0.01% residual porosity for optical transparency. Scientists compared both conventional and modern processing techniques for transparent ceramic materials, the findings shows that modern processing techniques were better in morphological/mechanical properties. Consequently, the major drawbacks experienced during the consolidation processes can be attributed to the chemical impurity of sintering methods, the ceramic or the processing flexibility of the ceramic, sintering aids employed, and microstructural characteristics (e.g., porosity). In this review, an effort was made to

---

* Corresponding author.
E-mail address: akinribideojo@yahoo.com (O.J. Akinribide).

https://doi.org/10.1016/j.jmrt.2022.09.027

summarize the advancement of transparent YSZ ceramics, focusing on applications and various consolidation technologies.

1. Introduction

The demand for innovative materials with required economic viability, cost-efficiency, and higher tolerances has paved the way for new optical elements for fabrication. This is achieved by applying advanced manufacturing materials and technologies. Nowadays, transparent ceramics are promising as optimistic single-crystal in-house materials and single-crystal technologies due to their photonic quality, particularly for optical applications according to Xiao et al. and Saghir et al. [1,2]. They also fill the gap for intelligent applications such as highly durable visual materials employed in harsh and extreme conditions where glass cannot resist. Furthermore, transparent ceramics are more versatile and economically viable than conventional transparent materials with unsteady chemical stability and mechanical properties [1]. Owing to processing flexibility during large-scale manufacturing, this class of ceramic which is also known for its high refractive index has drawn a lot of attention in optical applications. It has contributed significantly to the reduction in the price of the final product [3]. Due to their crystal and electronic structure, there is a high potential to develop transparent materials using the oxides based technique. According to Kotaro Kawajiri et al. [4], recently, many investigations on indium tin oxide and aluminum zinc oxide have been tailored toward actualizing the fabrication techniques and technological properties of transparent ceramic oxides. Among these oxides, zirconia (ZrO_2) has been extensively employed in innumerable fields of science and engineering technologies due to its outstanding performance and increased life expectancy. High microhardness, impact resistance, low thermal conductivity, and chemical stability which could rise to 2000 °C are among the mechanical and functional qualities of this ceramic.

Research by Kong et al. [5] has proven that optical glasses and other ceramic oxides do not possess a refractive index of 2.2 compared to Cubic ZrO_2 [6]. However, zirconia exists in three distinguished crystal structures: cubic, tetragonal, and monoclinic forms, making it challenging to fabricate pure/undoped ZrO_2 ceramic parts at high temperatures. For cubic and tetragonal zirconia, stabilizers are employed. The sintering temperature of zirconia is estimated to be at ~1500 °C, where zirconia exists in the monoclinic phase. Some previous works [7–9] have also confirmed that some ceramic oxides, such as MgO, CaO, and Y_2O_3, can reduce the crystallographic structures of soluble ZrO_2. This transformation spans from tetragonal to monoclinic, including a cubic structure following the transformation temperatures. As reported in literature, the most widely used stabilizer for cubic and tetragonal phases of zirconia ceramics is yttrium oxide (Y_2O_3). This is owing to its mechanical strength and good optical characteristics [8,10]. ZrO_2 stabilized by Y_2O_3 in the cubic variations (YSZ) is regarded at the promising material for a wide range of fuel cells electrolytes. They are also used as oxygen sensors in many industrial uses.

Cubic YSZ ceramic shows a high refraction coefficient (~2.2), permitting chromatic deviations. Furthermore, the material possesses an immeasurable potential for instrument-building applications, primarily due to the transparency of electromagnetic radiation in large areas of wavelengths from millimeters to the near-infrared spectral region [11]. The transparency features must achieve total density and exceptionally low porosity. It is achieved with less than 0.01% residual porosity [11]. The most common method is sintering, an advanced technique used to fabricate transparent YSZ ceramics due to their elevated melting temperatures. For high-density consolidation of YSZ, sintering technologies such as hot pressure (HP), hot isostatic pressure (HIP), vacuum sintering, microwave sintering and spark plasma sintering (SPS) have been employed [11–14]. Sintering aids and a combination of sintering techniques have also been used to improve the optical properties of this material [15]. However, visual defects such as grain growth [14] and residual pores [16] imposed by various sintering technologies have been reported. Transparent ceramics can be shaped using a wide range of powder metallurgy processes; however, previous results have been obtained. This paper presents a comprehensive review of the current state-of-the-art spark plasma sintering of advanced transparent ceramics and analyses of opportunities, issues, advantages, and limitations that often arise during advanced transparent YSZ Opto-ceramics processing.

2. Transparent ceramic materials

The capacity of a substance to allow the passage of light through it without scattering is known as the transparency or light transmission [17]. When a medium facilitates the production of an undistorted image, it is said to be transparent [18]. The light wavelength can either reflect [17], absorb, scatter, or refract light rays. Goldstein and Krell explained the dispersion and absorption as the two important factors that involve the most challenging processes to understand and avoid/reduce during the fabrication of transparent ceramics materials [17]. Translucent polycrystalline ceramics provide expense and manufacturing convenience benefits over single crystal ceramics. Nonetheless, the grain boundary involvement and pores in polycrystalline ceramics lower transparency and make sintering densification difficult [19]. Several techniques have been used for the fabrication of transparent and translucent ceramic materials, however, high-pressure (HP), high isostatic pressure (HIP), vacuum sintering (VS), and spark plasma sintering (SPS) are only a few of the sintering techniques that have been adopted for the fabrication of transparent ceramics from powdered precursor material [3,5,20]. Pressure-operated procedures, out of all of them, require the most control over experimental factors, such as high temperature, pressure, and sintering time, and these processes are frequently aided by undesirable rapid grain development that reduces transparency. The first experimental demonstration of CW laser-induced crystallization on tellurite glass with the formula 10RO-10Sm2O3–80TeO2 (R = Mg, or Ba) was carried out by Komatsu et al. [21,22]. Only 30 s of exposure to a continuous wave YAG:Nd laser at 1064 nm produced Sm2Te6O15 crystal dot patterns with diameters of about 50–150 nm. The authors linked the crystallization behaviours to the presence of Sm3^{+} ions since they have considerable absorption near the irradiation source (1000 nm), and no crystallization was seen when Sm_2O_3 was substituted for Er^2O_3. When annealing tellurite and germanate-based glasses, Goutaland et al. [23] employed CW UV-laser irradiation and discovered that the incorporation of the active ion (Er3+) into the crystalline phase is increased compared to standard thermal annealing.

Transparent glass-ceramics were lately being prepared using the spark plasma sintering (SPS) process. With the use of an extremely sophisticated technique called the SPS, highly homogeneous transparent glass-ceramics with extremely intricate nanostructures may be created quickly for optical applications. Other techniques used include auto-ignited modified combustion technique: The modified combustion technique is a remarkably easy way for producing phase-pure nanoparticles of transparent ceramic materials with good sinterability without subjecting them to extended high-temperature calcination. The combustion method differs from other fabrication procedures due to its quick processing time, ability to produce products with a high degree of purity, low production costs, etc. [24,25]. Research has proven that $MgAl_2O_4$ with a nanostructured size is prepared using an auto-igniting combustion synthesis in a single step by Thomas et al. [26]. The XPERT-PRO X-ray diffractometer which uses X-ray diffraction (XRD) was used to characterize as-prepared samples and determine the crystalline structure and phase of the nanomaterials. Using a Shimadzu spectrophotometer, the spinel nanoparticle samples are measured as-prepared (UV-1700). By employing a Perkin–Elmer spectrum two Fourier Transform Infrared spectrometer (FTIR) in the 400–4000 cm^{-1} range and the KBr pellet method, the phase purity of the material is confirmed. Utilizing transmission electron microscopy, the combustion product's particulate characteristics are analyzed by (TEM, Model-Hitachi H600 Japan).

Doping and fast sintering methods: Transparent ceramic materials are further improved in efficiency by doping and rapid sintering techniques. The effectiveness of infrared transparent window material is decreased by the presence of pores. The ceramic must have optically flawless crystal borders and crystals in order to be transparent. Because the surface of a pore represents a transition point between phases with radically differing optical characteristics, it strongly reflects and refracts light. Ceramics are opaque because they have a lot of pores. Intercrystalline or intracrystalline holes are also possible [25]. The huge grain size is a result of high-temperature sintering that occurs above 1600 °C. This is due to the fact that the material needs to enlarge its grain size during recrystallization and recovery in order to produce internal energy. Consequently, producing exceptionally dense transparent ceramic material with low pore content is quite difficult [27].

Microwave sintering method: High-density, transparent ceramic materials are manufactured using the microwave sintering process, which compacts the powder to an ideal density at a lower temperature without significantly reducing the material characteristics of the sample. The microwave sintering method significantly reduces the porosity. Despite the fact that there are numerous methods for manufacturing highly dense infrared transparent ceramic materials, all of them require hot isostatic pressing [28–30] or sintering additives [31,32], which also help prevent material loss [33,34]. To eliminate the intercrystalline and intracrystalline pores in every other procedure, an additive is required [25], but in the current work, utilizing a microwave sintering technique, They are able to significantly reduce the pores without additives.

A schematic indicating the light interaction sites for a microstructure of polycrystalline ceramic is shown in Fig. 1 below; the diagram has an incident intensity (I0), as well as a diffuse reflection (RD) and diffuse transmission component to the light (IDT) is formed based on the surface roughness. Additionally, specular reflection (RT 13%) reflects a portion of the light on each material surface. Pores with residual scattering over the grain boundaries could light polycrystalline transfer materials, particularly when considering the secondary phase. Unwanted materials could also serve as an inclusion absorption or as anacattering birefringence (non-cubic crystallographic phases of refracted rays). Because it is simple and scalable, the solid-state reaction approach is more cost-effective than other methods for measuring transparent ceramic materials. Solid–state processes involve solid precursors, sample homogeneity can be a severe problem.

2.1. Metal oxides

The application of metal oxides is similar to inorganic materials in sensor and biosensor applications [36,37]. Literature has proved this existence in different applications such as volatile organic compounds and toxic gases [36]. In the ceramic glazes, natural raw materials, metal oxides, or specifically created pigments of inorganic materials are also applied. Metal-oxides possessing different raw materials can be heat treated at high temperatures 2050 ± 53 °C to produce inorganic pigments. Dyes that are not soluble can easily be dispersed as tiny particles in their crystal structures in the glaze composition without degrading [36]. Iron oxide is one of the most often used metal oxide due to its excellent thermal stability, brightness in terms of intensity and stability in chemical properties [38–40]. It has a vital melting feature in addition to the iron oxide produce distinct forms on the glaze surface depending on the degree of aggregation. Crystal nuclei appear in bundles on glaze surfaces due to the extended cooling period in metal oxide glazes, increased temperature, speed up crystal formation in the glaze, and big crystals develop after cooling. Crystal formations may be visible on the product surfaces, and crystals that cover the surface can be created, [41,42].

Phosphorescent glass-ceramics have lately been recognized due to their unusual optical data processing and protracted (OPP) capabilities and have sparked a lot of attention [43–46]. Trap centers, where emission and radiance intensity, are primarily responsible for OPP. The development of the traps centres has been attributed to the doping of glass structures and various metal-containing transition ions. The defect experienced in the crystallographic structure has been traced to some dopants. [47–49], which is the primary cause of optical data processing and protracted OPP [49–51]. Impurity defects form trap centres, which leads to the phenomena of optical data processing and protracted OPP. Various research had concentrated upon the substrate material with various rare earth and transition metal ions, notably RE ions, which have a broad spectrum range from ultraviolet to visible, as a source for centre imperfections, making them useful in lighting and displayer equipment [52].

2.2. *Aluminum oxide*

The lightweight properties of aluminium oxide is one of the contributing factor, making it one of the widely used materials for different engineering applications. Corundum (Al_2O_3), diaspore (Al_2O_3 H_2O), gibbsite (Al_2O_3 $3H_2O$), and bauxite are some of the minerals derived from alumina. One other naturally occurring formation of alumina is corundum, which is made up of small quantities of impurities and gives valuable stones like ruby and sapphire their kinds. The three most prominent drives for alumina are 1. As an active oxide for chemical process, 2. As-received materials for most experimental work and 3. For metal production. Aluminum for industrial ceramics, and chemical processing all employ bauxite-derived aluminum oxides in various forms.

Corundum, ruby, and sapphire are mineral gemstones., on the other hand, are described as alumina [53].

2.2.1. *Different combination of alumina (Al_2O_3) as oxide ceramics*

The application of Alumina in the production of transparent ceramic materials has attracted much interest because of improved properties such as the thermal and the mechanical over their parent glasses, transparent glass-ceramics (TGCs) have gotten a lot of attention. Transparent glass-ceramics possess the unique features of glasses and transparent ceramics such as high impact resistance, high strength, low thermal expansion coefficients, occasionally even negative thermal expansion coefficients. They are even better than glasses and transparent ceramics due to the reduced scattering loss. TGCs have been made from alumina silicate glass systems, including $Li_2O-Al_2O_3-SiO_2$ [54], $ZnO-Al_2O_3-SiO_2$ [55], $MgO-Al_2O_3-SiO_2$ [56], $CaO-Al_2O_3-SiO_2$ [57], and others. At the same time, only a little study has been done on the optical characteristics of Na2O− Al2O3−SiO2 glass-ceramics [58] and dental uses [59]. $Na_2O-Al_2O_3-SiO_2$ glass-ceramics containing nepheline ($NaAlSiO_4$) as crystalline phase has produced for the manufacturing of microwave ovens [60] also in medical applications such as dentistry [61].

Inorganic compositions comprising metallic or metalloid substances containing oxygen are known as oxide ceramics. They are suitable for an extended application because of their superior mechanical performance, corrosion resistance, and wear properties. Oxides can resist even the most demanding industrial processes and applications since they have the highest oxidation state of all metals. The use of transparent ceramic for bone implant prosthesis has been proposed, and oxide ceramics have been found to be biocompatible. Alumina (Al_2O_3) has aroused the interest of ceramic biomaterials due to their stiffness and compatibility with the human body system [62].

This type of ceramic is generally not visible due to crystal dispersion in the matrix. When manufacturing transparent glass-ceramics, a minimum of light is needed for transmission [63,64]. To induce crystallization, several nucleating agents, such as TiO_2, ZrO_2, Cr2O$_3$, or LiF, are added to $Na_2O-Al_2O_3-SiO_2$ glass to produce nepheline glass-ceramics [58]. High mechanical strength glass-ceramics may be obtained by the controlled precipitation of nepheline crystals in glass, and applications in dental porcelain [59,60], and dinnerware [59] have been developed. There is a strong reduction in chemical composition when considering high-level waste glass-ceramic for long-term durability, and this reduction is driven by the uncontrolled precipitation of nepheline crystals, since each mole of Na2O removes three moles of glass formers (1 mol Al2O3 and 2 mol SiO2) from the amorphous network. As a result, understanding the crystallization process of $Na_2O-Al_2O_3-SiO_2$ glasses is critical. [65], and [66], respectively.

2.3. *Zinc oxide*

ZnO is a multifunctional material with several intriguing features, such as UV absorbance and other importance as the case may be are all features of this material [67]. In addition, ZnO comes in a range of particle shapes that impact its capabilities and define its possible uses in various technologies, it can be manufactured in the laboratory by electrolyzing a sodium bicarbonate solution with a zinc anode. Hydrogen gas and zinc hydroxide are generated when heated zinc hydroxide decomposes to zinc oxide [$Zn + 2H_2O$ $Zn(OH)_2 + H$]. Owing to its disinfecting, antibacterial, and drying qualities, ZnO has found usage in the design of different variety of medications [68,69]. Part of its application include its usage as drug for epilepsy and diarrhoea disease, and it is currently found in ointments and creams and in liquid powders [70]. The powder form of liquid ZnO is also utilized in dermatological treatments to relieve itching and irritation while expediting wound healing [70]. It is also used in dentistry as a component of dental pastes and for temporary fillings. ZnO is employed in a range of nutritional items and diet supplements because it may provide vital dietary Zn [71,72]. The adhesive nature of ZnO is very low compared to other transparent ceramic materials, making the complete removal of all the disadvantages. These NPs' distinctive properties, such as UV radiation absorption, skin non-irritation, and the ability to penetrate fast into the skin, make them stand out for these characteristics.

2.4. *Magnesia (MgO)*

With the advancement of civilization and technology, the need for novel materials with different physical and chemical qualities has increased. This has promoted the use of magnesia which is also a translucent material. It has FCC crystalline structure, and a low density (3.50–3.58 g cm^3) at ambient pressure and is elevated around 3123 K, with poor thermal conductivity 30 W m^{-1} K^{-1} down to 8 W m^{-1} K^{-1} and good mechanical properties. The energy band-gap of MgO is relatively wide (7.8 eV) and is an excellent insulator [73,74]. Pressureless sintering, hot isostatic pressing (HIP), hot pressing additives, and spark plasma sintering have been reportedly utilized for the fabrication of fully transparent MgO ceramic [73,75,76]. Sintering procedures are equally significant for lowering sintering temperatures and improving ceramic transparency. Reduction in the sintering temperature can be attributed to densification aids. However, researchers have shown that this negatively impacts the optical properties. Work by Itatani [77] demonstrated that using post-HIP, translucent Magnesium oxide ceramics can be produced at a relatively high temperature of about 1600 °C without needing a sintering aid such as post hot isostatic pressing).

In the IR region, the spectra of the in-line transmission of MgO specimens with 0.5 h of hot isostatic pressing at 1600 °C after considering pressureless sintering at 1600 °C intended for 5 h rose by 55%. MgO crystals were found to have higher transparency. By hot-pressing transparent MgO ceramics with LiF additive, Fang et al. [78] created translucent MgO ceramics. Varying parameters such as time and pressure have been considered in the hot-pressing of transparent ceramic materials in argon and vacuum environments, as the specimens in the environment appeared to be thick and translucent. Another study by G Ling et al. [79] was carried out by using pressureless sintering at a temperature of 1400 °C for 2 h. SPS has grown in popularity as a novel way to sinter magnesium oxide. After SPS, Kato got a translucent bulk sample. The MgO ceramic has a VIS transmittance of 20–50% and an increase in transmittance in the IR spectrum [80].

2.4.1. *Zirconium dioxide*

Zirconia bioceramic is used as a structural ceramic in place of Al_2O_3 due to its significantly better fracture toughness and optical application as reinforcement in ceramic based composites. Any monolithic ceramic with the maximum fracture toughness value is ZrO_2. Polymorphism is a feature of zirconia ceramics that allows them to undergo several changes after different stages of cooling to ambient temperature. ZrO_2 contains three unique polymorphs, including crystallographic face from mono, tri and tetragonal. The transitions to the tetragonal phase above 1170 °C (Tss-tetragonal solid-solution phase). If is stable up to this temperature, the cubic phase solid-solution phase) appears above 2370 °C and lasts until 2680 °C, when it melts. When it cools from the tetragonal to the monoclinic phase, it displays a considerable volume change of 3–5% [81].

In comparison to other ceramics, ZrO_2 metal oxide ceramics have reduced hardness and modulus of elasticity due to their high density and stiffness [81]. Research has shown that the most significant application of zirconia in the health sector is bone or hip replacement. In terms of osteointegration and biocompatibility, the results of ZrO_2 implant applications were comparable to Ti implants. Furthermore, ZrO_2 possesses exfacesional qualities such as a great attraction for bone tissue noncarcinogenic properties. It also has no carcinogenic impact, making it a great choice for various implant applications. ZrO_2 grains might also serve to produce materials that contain carbon as nucleation sites, especially crucial to keep in mind when developing hydroxyapatite as implant materials. In Contrast to ZrO_2, Al_2O_3 has does not attract Ca or H from ions derived from phosphate. Cauliflower-like calcium phosphate mineral growth was seen to spread across the gap and throughout the whole ZrO_2 surface [82].

2.4.2. *Manganese oxide*

Due to their unusual physical and chemical features, manganese oxide nanoparticles (MONs) such as MnO, MnO_2, Mn_2O_3, and Mn_3O_4 have received much attention from scientist of rand recent [83]. Due to their adaptable architectures and morphologies, they seem to have a lot of potential for medicinal applications Rockenberger et al. scientists a thermal breakdown approach to make monodisperse colloidal Mn_3O_4 NPs. For MRI of live beings, as induced magnetic resonance contrast agents [84]. MONs were increasingly exploited as optimal response to some microenvironment [85]. Other less frequent synthetic techniques have been reported, including the laser ablation approach, polyol-type procedure, and one-pot microwave synthesis [84].

2.5. *Processing of transparent MgO*

Recently, Kruk et al., 2018 researched on arc plasma synthesis of high-transparent Magnesium oxide ceramics [86]. From his experimentation, he obtained an MgO powder at the initial stage of the material. Ball milling technique was adopted as the first preparation method with thorough mixing within 0.5 h with a zirconium mortar before being dried for 4.5 h in an enclosed oven furnace at the temperature of 85 °C. The As-received, the powder sample was then biaxially pressed into green bodies at an 80 MPa pressure. The melting process does not need nanopowders, which is another merit of this technique. Lastly, in the first few seconds, the samples were cooled at a 20 °C/s. The bulk MgO sample fabricated exhibited irregular forms and a thickness that is approximately 1 mm. A photograph of arc plasma burned MgO pellets is displayed in Fig. 2. Screens, aircraft windows, ballistic shields, transparent weapons and armour, and strong laser composites are just a few of the applications magnesium oxides. As a result, it's a good choice for optical materials.

2.6. *Transparent yttria stabilized zirconia for optical neuroimaging and other applications*

Transparent cranial implants might be a game-changer for laser-based with a large spectrum of diagnosis and deep treatment under good nervous conditions. Nevertheless, catastrophic fracture failures were noticed, causing severe limitations to transparent ceramic glasses due to the inherent brittleness of transparent implants, leading to a reduction in clinical translation opportunities. The utilization of ceramic materials known as zirconia were observed as a strong ceramic with well-proven biocompatibility in chronic implantation applications; this is widely used in the development of novel nanocrystalline transparent implants [87]. The typical crystallographically feature of Yttria-stabilized zirconia (YSZ) is shown below in Fig. 3;

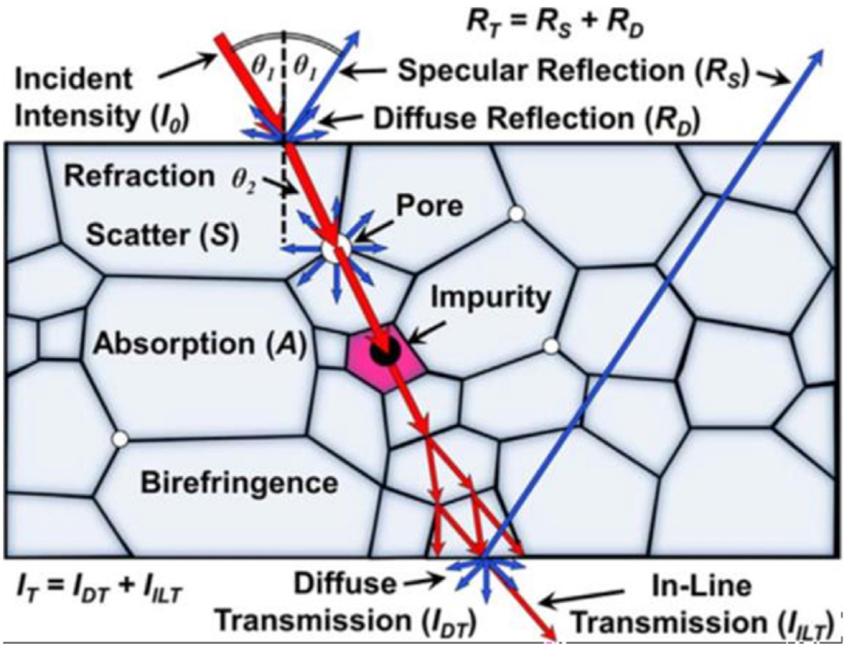

Fig. 1 – A schematic indication of the light transmission in a polycrystalline ceramic [19,35].

Optics ceramic materials have been used in the fabrication of infrared windows, domes, inspection ports, and other structures [88]. A heat-seeking missile uses a specially crafted infrared window that can follow its trajectory to detect the infrared radiation released by a target jet or spaceship exhaust. A multitude of military and commercial applications have made optical ceramic their choice material because of its superior optical transparency, strength, and hardness.

Among these applications are:

1. Windows and domes (UV, Visible, IR, and millimeter Wavelengths)

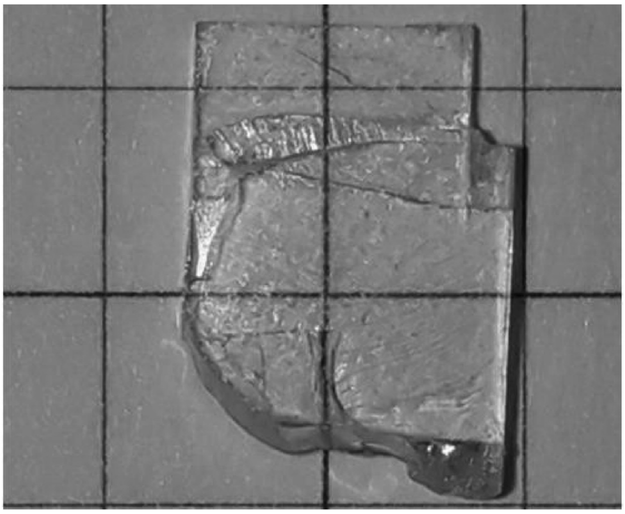

Fig. 2 – An image taken after polishing, transparent MgO was seen at room temperature a) and 405 nm UV b) light [86].

2. Transparent armor
3. Point of Sale (POS) Scanner Windows
4. Ceramic for semiconductor processing equipment
5. Low cost alternative to sapphire
6. Transparent alternative to alumina
7. Etch resistant alternative to quartz are some of the areas of applications [88].

2.7. *Significance of transparent zirconia ceramic glass*

Research has proven zirconia to be the most globally used ceramic material for optical and biomedical applications. This is owing to its unique properties both in the physical and chemical processes. For example, one of the main reasons for zirconia suitability as ball milling materials, cutleries, and mechanical bearing is its excellent mechanical and tribological properties [89]. For over a decade, zirconia has found good use in medical applications such as prosthetic dentistry for producing partial dentures and crowns [90]. The oxides of zirconia-based ceramic are also useful in the health sector, mainly in the prosthetic dentistry section for the development of fixed partial dentures and crowns [91,92]. Researchers have discovered the biocompatibility and aesthetic appeal as significant properties attributed to ZrO_2. The recent discovery of smartphones with 5G compliance has opened the floor for diverse applications of ZrO_2 in different areas such as fingerprint due to their sensitivity to touch, insignificant signal shield, and durability in the area of tribology [93,94].

Not until around 1975 recently, ZrO_2 was mostly employed as a refractory material, with little interest. This is owing to the phase transition from one noticeable to another i. e t –m of ZrO_2 phases. The disorderly segment change is complemented by 0.16 shear strain and a 4% volume increase that

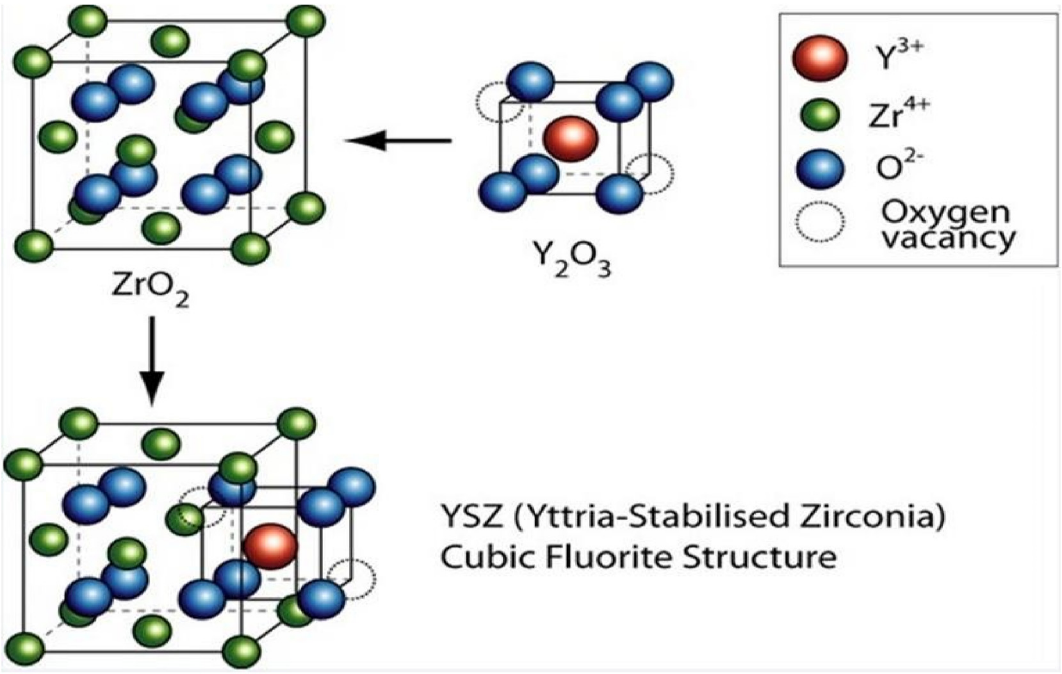

Fig. 3 – Yttria-stabilized zirconia (YSZ) crystal structure [87].

might result in disastrous ZrO_2 rupture. The revelation that rigorous structural control can adequately manage the t-ZrO_2 to m–ZrO_2 transition [95] has resulted in the most significant rise in its industrial usefulness. When the ceramic is loaded at ambient temperature, metastable t- ZrO_2 may be stabilized, and it converts to m-ZrO_2. The following volume expansion might effectively inhibit the formation of fractures, resulting in improved stiffness. It can also be described as "phase transformation toughening" [95,96]. The dopant distribution in glass-ceramic is fascinating because dopant(s) may be found in four distinct places: inside ZrO_2 nanocrystallites, in the SiO_2 matrix, at the ZrO_2 grain boundary, and at the ZrO_2/SiO_2 heterophase interface.

Recent research by Fu, L. et al., 2020 [97] shows that adding 3% mole of Y_2O_3 dopant, part of the Y_2O_3, which is Y fractional part was soluble in ZrO_2 and later found distributed around the grain boundaries. Segregation of the component Y fraction were also found segregated around the interfacial boundaries of ZrO_2/SiO_2 in Y_2O_3 heterophase. The result shows no significant traces of Y dopant in the matrix of SiO_2. Preceding results showed some Y_2O_3 dopant when 3% mole was applied, some fraction was also found dissolving in the zirconia nanocrystalline materials and separated as a bulk sample. In the SiO_2 matrix, there were hardly any Y elements. Table 1 show some specific information on properties and fundamental features of transparent ceramic oxides.

2.8. *Specific functions and features of transparent ceramic oxides*

Table 2 provides illustrative examples of the production of transparent ceramics. In particular, Mizuta et al. generated fine-grained transparent ceramics with in-line

Table 1 – Physical properties and fundamental features of transparent ceramic oxide.

Chemical formula	Crystal structure	Lattice constant	Thermal conductivity (Wm)	Density (g/cm3)	Tm (°C)	Tb (°C)	Ref.
ZrO_2	Cubic	a = 5.143 Å, b = 5.194 Å c = 5.298 Å β = 99.218° a = 5.094 Å, b = 5.174 Å a = 5.105 Å	123.22	5.68	2715	4300	[98]
Y_2O_3	Cubic (bixbyite), cI80	a = 10.6 Å	225.81	5.01	2425	4300	[99]
Sc_2O_3	Bixbyite	a = 9.84 Å	138.20	3.86	2485	–	[90]
Lu_2O_3	cubic	a = 10.393 Å	397.93	9.50	2510	–	[100]
$Y_3Al_5O1_2$	Cubic	a = 12.02 Å	593.70	4.55	1950	–	[101]

Table 2 – Optical transmittance and characteristics of transparent ceramic oxides.

Serial number	Powder processing techniques	Transmittance together with processing parameters	Ref.
1.	Precipitation-derived Y_2O_3	CIP: 200 MPa Calcination: 1100 °C/4 h 1700 °C/1 h vacuum sintering	[93,102]
2.	Co-precipitation and combustion produce Er:Y_2O_3	CIP: 200 MPa Calcination: 900–1100 °C/4 h 1700 °C/4 h vacuum sintering Vacuum: 105 Pa	[103]
3.	Carbonate precipitation yields Y_2O_3	1100 °C/4 h calcination Vacuum sintering: 1700 °C/4 h Heating rate: 200 °C/h 103.3 Pa vacuum, transmittance of 79% at 600 nm	[104]
4.	Coprecipitation produces 10% La_2O_3-doped Y_2O_3	CIP: 200 MPa Calcination: 900 °C/4 h Sintering in three stages: T1 = 1450 °C/0 h; T2 = 900 °C/20 h; T3 = 1700 °C 5103 Pa (vacuum), transmittance of 80% at 600 nm	[105]
5.	Slip casting with 5.0 mol% ZrO_2–Y_2O_3	900 °C/2 h calcination 1860 °C/8h Vacuum: 2103 Pa Vacuum sintering: transmitted 80% at 600 nm	[106]
6.	Solid-state reaction of ZrO_2– Y_2O_3 at 5.0 mol%	HP: 16001700 °C/3 h Pressure: 2040 MPa Calcination: 800 °C/8 h 9103 Pa (vacuum) 1200 °C/2 h post-annealing, transmittance of 76% at 600 nm	[107]
7.	Commercial Y_2O_3 nanopowder	1650 °C/6 h, 203 MPa HIP transmittance of 50% at 450–1100 nm	[108]
8.	Precipitation-derived Y_2O_3	Thermal decomposition: 1300 °C for 3 h CIP: 200 MPa for 5 min 1500-1400 °C/4 h pre- sintering 1600 °C/3 h, 200 MPa HIP of 73% at 600 nm transmittance.	[109]
9.	Tenth percent Commercial ZrO_2–Y_2O_3 powder	200 MPa CIP Vacuum sintering: 1600–1800 °C/5 h Vacuum: 11003 Pa HIP: 1600 °C/3 h, 200 MPa transmittance of 75 percent at 700 nm Vacuum sintering: 1600–1800 °C/5 h Vacuum: 11003 Pa	[109]
10.	Commercial Y_2O_3 powder	950–1050 °C/08 h Spark plasma sintered Heating rate: 2 °C/min at 1000 nm, 55 percent	[27]
11.	Precipitation produces Sc_2O_3.	1700 °C/4 h vacuum sintering Vacuum: 1103 Pa 60 percent at 600 nm.	[110]
12.	Coprecipitation of Eu:Lu_2O_3	CIP: 200 MPa Calcination: 1000 °C/2 h Sintering time: 6 h at 1850 °C At 600 nm, H2 makes up 80% of the atmosphere.	[111]
13.	Commercial Nd:Lu_2O_3 powder	1400 °C/15 min Spark plasma sintered Pressure: 130 MPa 75 percent at 650 nm Heating rate: 100 °C/h	[112,113]
14.	Zirconium dioxide ZrO_2	The film layers of ZrO 2 were synthesized by magnetron sputtering at various argon partial pressure values, with a maximum transmission of 80% from 300 to 800 nm.	[114]

transmittance up to 46% and mechanical strength of 600–800 MPa utilizing hot isostatic pressing (HIP) in conjunction with a vacuum–pressure slip–casting process. The green bodies were presintered in air at 1240 °C for 2 h at rates of 40 °C/min and 5 °C/min for heating and cooling, respectively. The sintered samples underwent additional HIP treatment at 1050–1400 °C for 1 h at 150 MPa. Heating rates for HIP were 30 °C per minute up to 500 °C, 20 °C per minute up to 1050 °C, and 10 °C per minute up to the final sintering temperature. Above 500 °C, pressure was increased at a rate of 3.4 MPa per minute. After sintering at 1350 °C and reaching 46% transparency, samples typically showed their highest transparency.

3. Basic optical transmittance and specific functions of transparent ceramic oxides

.

4. Various consolidation techniques for transparent ceramics materials

The process of transparent ceramics includes post-treatment operation, precursor powder synthesis, compacting and calcination/sintering, which is similar to that of ordinary ceramics (annealing, machining and polishing). On the other hand, transparent ceramics have unique needs, particularly in terms of powder synthesis and sintering. The transparent ceramic powder has the same synthesis method as high-quality powders when applying sintering techniques, such as hot pressing (HP), which is a powder metallurgical procedure that combines high pressure and low strain rates to generate powder compact at a high temperature able to fully initiate sintering and creep processes., hot iso-pressing (HIP) which is the sintering technique adopted wherein the powder is subjected to an isotropic compressed gas and during the heating process, resulting in good densification caused by the accumulation of high pressure and high temperature, vacuum sintering embraces the production of oxygen vacancies in the material, the material darkens and its effect on the optical properties are known, spark plasma sintering (SPS), and microwave sintering [3].

1. Sintering at hot pressing (HP)

HP known as the hot pressure sintering is a sintering technique in powder metallurgy that works with low strain rate at high pressure to synthesize powder at high temperature capable of inducing sintering and creep process in Fig. 4. The technique work with heat and pressure simultaneously. There is particle interface and plastic flow reordering, which make high-pressure densification works. This route is mostly used to generate brittle as well as hard materials. Due to this, HP route has emerged as a major method for producing transparent ceramics.

2. Sintering at high isobaric pressing (HIP)

The industrial method of HIP has been channelled towards minimizing metal porosity and improving the density of different ceramic materials. High pressure and isostatic pressure in Fig. 5 has been the means of exposing components in a high-pressure containment vessel. A sudden increase in the value of pressure in the vessel chamber was attributed to the heat generated from the chamber. A similar gas pumping could only be attained if sufficient pressure level and the system are achieved and the materials depend on the incoming pressure from all corners. The higher the materials is compressed or heated isostatically (HIPed) the more the densification possibilities, which is essential for good light transmission. Hot isostatic pressing is typically used as the final step to reduce fabrication costs, despite the fact that it has been proven to be a critical step in the preparation of ceramic with the good transparent ceramic duo to the high cost of production experienced while working with hot isostatic pressing sintering which prompts the importance of adopting dedicated equipment and experimental surroundings.

Considering the low-temperature high-pressure (LTHP) sintering studies, a diagram representation of the sample assemblage portion is shown in Fig. 5.

Alumina, Spinel as typical ceramic armour with transparent properties Transparent armour ceramics such as alumina have been synthesized using the HIP technique.

3. Vacuum sintering

The term “vacuum sintering” in Fig. 6 is mainly regarded as sintering techniques operating in a vacuum to produce improved outcomes than those carried out at normal pressure. Garnet made of transparent and rare-earth sesquioxide ceramics, such as Y_2O_3 and Sc_2O_3 [131,132], are often made by vacuum sintering. When fabricating YAG ceramics using vacuum sintering, the technique commonly involves using air annealing [115].

4. Spark plasma sintering

SPS is a recently discovered process utilized for the production of complete transparent ceramic materials with fine grains and dense compaction at low temperatures, within a short period of time. This is also known as pulsed electric current or field-assisted sintering. Fig. 7 shows a schematic design of SPS. Normal hot pressing involves heating a coil from the outside, whereas SPS involves flux with high-density current running between the die as well as the sample to generate Joule heating within the sample. SPS has a substantial advantage over HIP and HP in that it can accomplish powder consolidation in a short amount of time [117]. As a result, it increases the density of powders without causing grain coarsening, which is unavoidable in other densification methods. The densification process is categorized into three steps [29]. The first step is defined by particle packing followed by the associated process of diffusion with grain sliding and neck development. The third stage is characterized by the pores elimination process mostly along the grain boundary. The process of densification and packing initiation at the second and third phases are substantially influenced by the applied pressure.

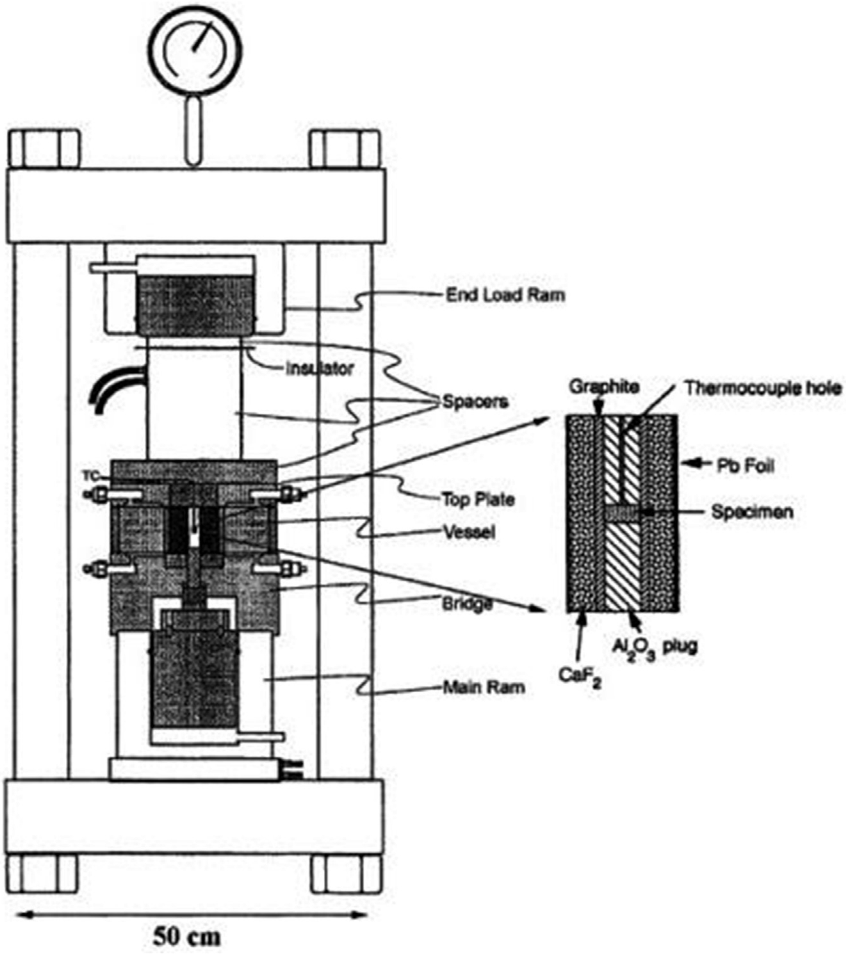

Fig. 4 – Shows the schematic sketch of high pressure sintering using high temperature [3].

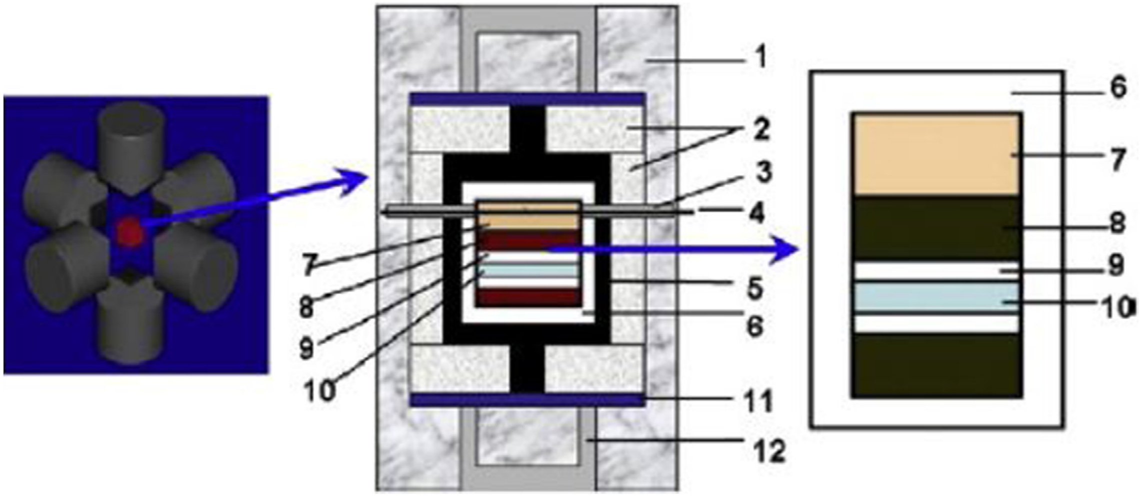

Fig. 5 – Shows a typical representation of the hot isostatic pressing HIP with the following labelling for each parts; 1. pyrophyllite, 2. dolomite, 3. Ceramic tube, 4. Thermocouples, 5. Graphite heater, 6 NaCl capsules, 7. hBN, 8. WC substrate, 9. NaCl sheet, 10. Sample, 11. Mo sheet, and 12 steel heater [3].

Fig. 6 – Vacuum sintering plant [116].

In a typical SPS process, a high pressure is applied continuously. Another essential sintering characteristic for densification in the second and third phases is heating rate. .

5. Microstructures, TEM images and EDS analysis of transparent ceramics materials

Using the wet shaping approach and hot isostatic pressing, research has shown that scientists were able to successfully manufacture Er3+ doped transparent alumina (0.1–0.17%) with visible light photoluminescence. On the final microstructure, definite in-line transmittance, and photoluminescence properties, the impacts of dopant quantity, kind of doping powder, and powder pre-treatment were investigated in the research. Depending on the processing conditions, true in-line transmittance ranged from 28 to 56 percent. As the quantity of dopant was increased, the transparency dropped. The amount of reduction is determined on the type of doping powder used and its pre-treatment. Due to the presence of Er^{3+} ions, photoluminescence spectra in the visible and near-infrared regions displayed characteristic emission bands according to Drdlková et al. [118]. The Er_2O_3 powders were blended into the Al_2O_3 suspensions before drying for 5 h at room temperature and then another 5 h at 80 °C. All green bodies were pre-sintered using one of two techniques to produce 95–96% r. d with enclosed pores [118]. The single step pre-sintering SSP process consists of sample heated to a temperature of 1480 °C for 20 °C/min besides cooling them. The same sintered compacts were heated to 1430–1440 °C (T1) and later cooled near 1280 °C (T2) at 20 °C/min for 10 h. Hot isostatic pressure in argon environment was carried out at 1280 °C in addition to 200 MPa for 3 h. The TSP technique was shown to be more successful than the SSP process in producing high transparency Al2O3 ceramics.

The clear efficiency of Al_2O_3 was determined at high rated optical properties as demonstrated in Figs. 2 and 3. The illustration shown in Fig. 8 confirmed the morphological structure of SEM and TEM. The fabrication of transparent Al_2O_3 ceramics has always being done using spark plasma sintering (SPS) [119–122]. To change the grain size of transparent Al_2O_3 ceramics, Suarez et al., 2012 [123] employed SPS and a self-doping technique [75]. Furthermore, Schehl et al. [124] employed a colloidal approach to dope aluminum ethoxide into high-purity commercial Al_2O_3 nanopowder. To make slurries, there is a need for proper removal of ethanol

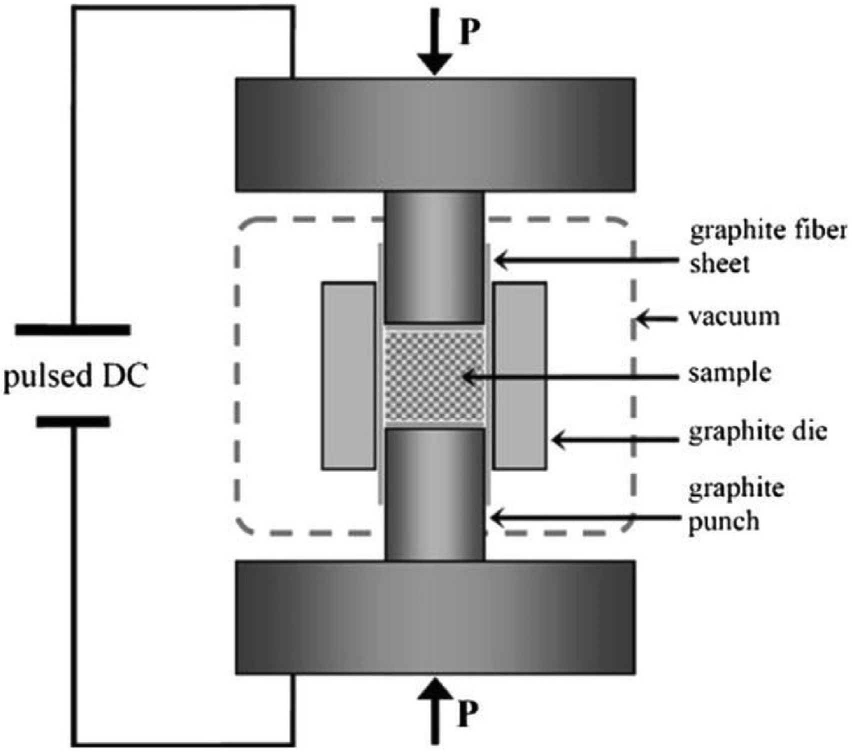

Fig. 7 – Diagrammatic representation of the spark plasma sintering process [3,113].

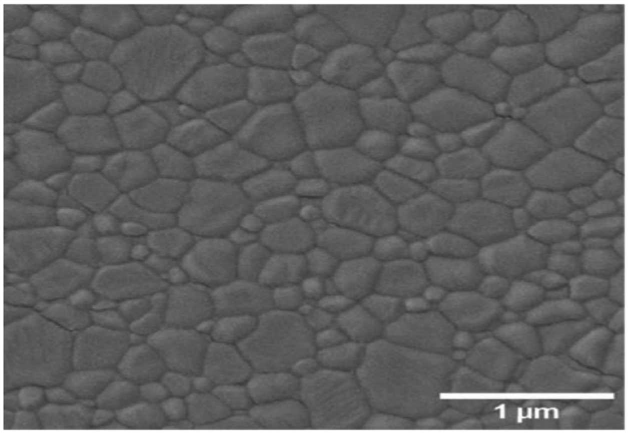

Fig. 8 – SEM image after HIP, of Er^{3+-} doped Al$_2$O$_3$ ceramics [1].

which prompted the precursor solution of aluminum ethoxide to dissolve anhydrous ethanol following the suspension of alumina in ethanol, the sample was allowed to dry at the temperature within the range of 60–70 °C, mixing was done thoroughly with the aid of magnetic agitation and dried at 120 °C in theair before the removal of ethanol. The powders were later forced into pellets at a uniaxial pressure of 30 kPa sintered at 1100–1400 °C for 0.5 h. For 100 °C/min, 80 MPa, and 0.1 mbar, altogether. The mechanism of Spark plasma sintering process was hindered by doping of atomic diffusion, which prompt the inducement of a transition from grain boundary to volume diffusion process and vice versa, permitting control of grain size refinement, particularly in the microstructure of the final ceramic materials. SPS Al2O3 also had a lower activation energy than conventional sintering, which was about 50% lower. Because the applied pressure forced the Al2O3 granules to rearrange themselves.

The pure and doped samples in Figs. 8 and 9 had identical microstructures before sintering; however, following sintering at 1100 °C for 30 min, considerable variations were found, as the pure samples exhibited strong level of densification with evident grain development, but the self-doped samples had essentially no grain growth. The Al$_2$O$_3$ nanoparticles adhered to huge particles surface in the doped samples and separated, altering the sintering behaviour. Not until the temperature reached 1340 °C, the expected density of the doped powders was not fully attained completion due to the energy barrier expected to rise by self-doping, which was observed to be roughly 50 °C above the as-received powder samples. The grain orientation was hampered in the starting phase of the sintering because of the nucleated particles existing in the doped samples. There is evidence of bigger grains observed in the undoped samples at sintering temperature 1300 °C even prior to diffusion of ions in the grain boundaries, which show the existence of full inhibition of Al$_2$O$_3$ grain growth, which is visible in form of grain size enlargement. The phases of sintering, since grain rearrangement governs sintering. During the first stages of development [125,126]. As a result, dopants are quite beneficial. .

5.1. *XRD studies on transparent ceramics*

Fig. 10 shows the patterns of X-ray diffractometer of the nanopowder particles called Pr:BaF$_2$ precursor as a transparent ceramics with variable content of Pr^{3+}, presence of a corresponding shift in the curves of the lattice parameter and cell volume for transparent ceramics were observed even along with different Pr^{3+} content. There is full evidence of cubic fluoride fundamental structures in all sample patterns, as shown in Fig. 10a, which are synonymous to the typical BaF2 phase (JCPDS: 04–0452). The peak of the impurity content remained undiscovered [126]. We also observed the effect of Pr-doping on the BaF2 crystal cell in Fig. 10b, with the sudden increase in the lattice constant and cell volume at first and thereafter progressively decreasing with an evident rise in the

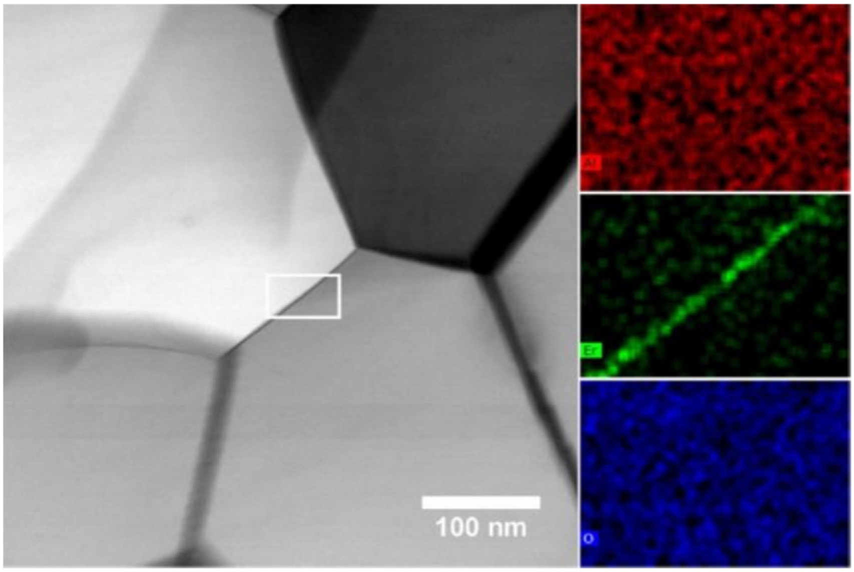

Fig. 9 – TEM picture and EDS profiles (Al, Er, O) of the 0.1 at percent Er3+-doped Al$_2$O$_3$ grain boundary [1].

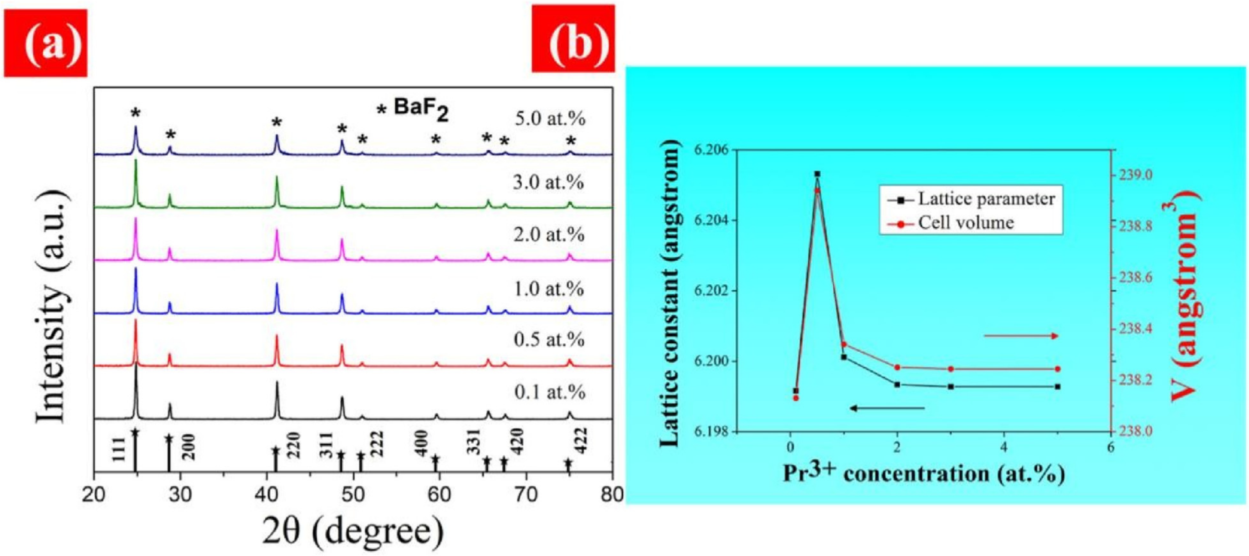

Fig. 10 – (a) The pattern of X-ray diffraction showing the ratio of xPr: BaF2 nanopowders, x = 0.001–0.05; (b) Lattice constant and space volume variations [113].

doping concentration. From the illustration, we observed that the lattice constant attained a peak of 6.205 nm at 0.5% Pr^{3+}.

In light of this, Zhou et al. [127] proposed a competitive connection that is common between lattice shrinkage, which mainly triggered by rare-earth ion additional performance (here, Pr^{3+}: 1.013) and substrate ion replacement behaviour (here, Ba^{2+}: 1.35) and because of non-equivalent effect observed, the filling of interstitial F- on barium fluoride lattice was seen as a non-equivalent replacement of the two ions, This is done with the mind of balancing the charges present. There is an need for an enlargement in the overall width of principal diffraction peaks even at half-maximum size, which is clearly shown from the XRD data from the rare earth doping concentration, suggesting some decrease in the level of crystallinity of the powder sample. The injection of ions causes lattice deformation, which causes this phenomenon.

5.2. *TEM and SEM images of transparent ceramics nanopowders*

Fig. 11 shows SEM images of various Pr^{3+} contents doped as-synthesized BaF2 nanopowders. Increase in the doping

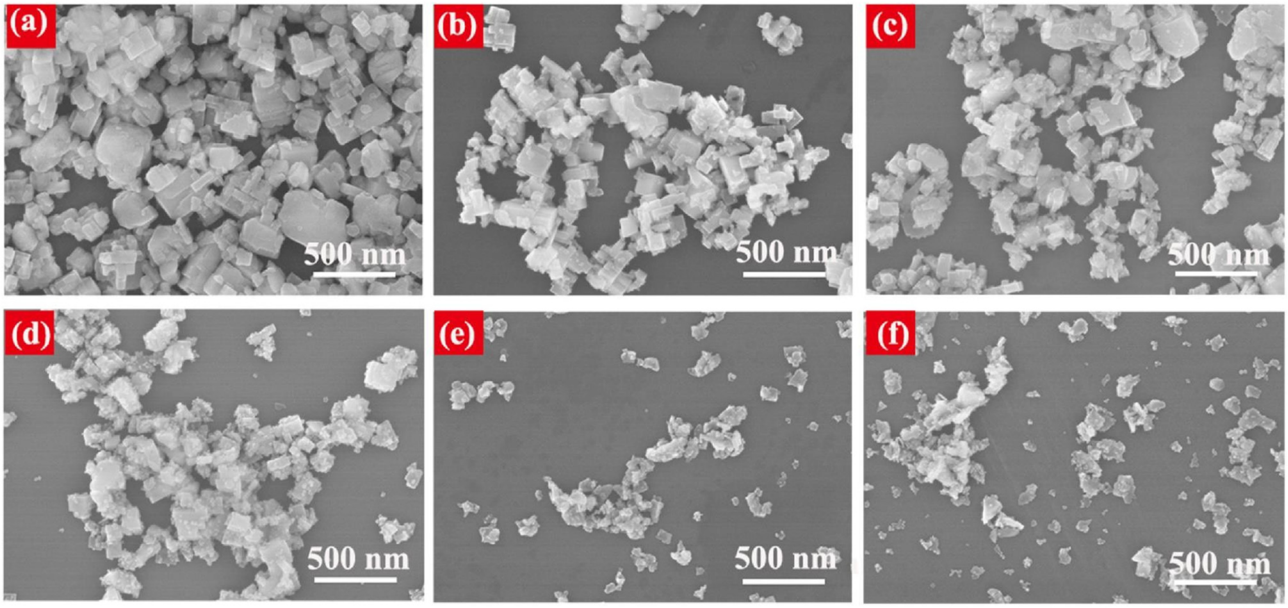

Fig. 11 – Shows the scanning electron microscopy images with secondary electron mode of xPr:BaF2 nanopowders; (a) x = 0.1 at 5%, (b) x = 0.5 at 5% (c) x = 1 per cent, (d) x = 2.0 per cent, (e) x = 3.0 per cent, and (f) x = 5.0 per cent [128].

concentration brings some agglomeration of powders increases, and the average particle size decreases considerably, as seen in Fig. 11a–f. Square geometric shapes of various sizes produced at less than 2% low doping doses. In Fig. 11d–f, the uniform square structure transforms into an irregular sheet shape, and small nano powder particles instigate to sprouting and growing observed. As hitherto stated, the discovery of a new interstitial site for F- usually emerge. The amount of this increases as the number of doping ions increases, which is permissible to maintain the solid solution structure's electrical neutrality. The following are two different defect equations:

$$PrF_3 \overset{BaF_2}{\rightarrow} Pr_{Ba} + 2F_f + F^{!}{}_{I} \tag{1}$$

$$2PrF_3 \rightarrow V^{!!}{}_{Ba+4Ff} + 2Pr_{Ba} \tag{2}$$

The impact of BaF2 on the microstructure and mechanical properties of the transparent ceramic glasses with Er3+/Yb3+ co-doped fluoro-tellurite glasses generated mostly by melt application of pressure is explored in depth. Using scanning electron microscopy bomb calorimeter and Spectroscopy machine, this transparent ceramic materials was discovered to have high thermal stability and minimal phonon energy.

The two defect response processes outlined Fig. 12 above are theoretically possible. However, if VBa is present, one-quarter negative ions charge of Ba^{2+} in each of the lattice, consisting $8F^{-}$, disrupting the crystal structure due to negative charge repulsion. Finally, the Ba1xPrxFx+2 solid solution forms the F- type. As the amount of Pr doped rises, there is an appreciable change in the corresponding size and shapes which eventually leads to a rise in the repulsive nature of the surface of the powder generated by the fluorine ions to promote additional dispersed nanopowders, and we also observed that the normal interstitial F- ion site scaled up as the amount of Pr doped increased. To fully comprehend the influence level of the doping nature of Pr^{3+} on the scope and structure of aimed BaF_2 powders, TEM findings between the two ranges of (0.1–5.0)% Pr-doped BaF_2 powders were clearly displayed in Fig. 12. There is a consistent mean size of over 100 nm, transforming into uneven sheets with a mean size of around 20 nm, as seen in Fig. 12a and b. The various powders' lattice fringes in Fig. 12a and b are reproduced in Fig. 12c and d, with an inset displaying the corresponding SAED pattern. The HRTEM micro magnification in Fig. 8c and d shows some spacing called culminated from the lattice structure of 0.355 nm and 0.293 nm, respectively, which correspond to the (111) and (200) facets of BaF_2 crystals [127].

5.3. *Crystallization behaviour*

XRD analysis of glasses such as SG, SE, and SN heat-treated for 5 h at varying temperatures (650–780 °C) for 20 °C intervals are shown in Fig. 13. With increasing heating temperatures, the crystalline phases of ZrO_2 (JCPDS No. 50–1089), low-carnegieite (JCPDS No. 52–1324), and nepheline (JCPDS No. 34–0424) precipitated sequentially gotten from the three selected glasses. The glass SG remained amorphous at 650 °C, with no diffraction peaks, there is a tendency for both SE and SN glasses to display peaks of diffraction gotten from the crystal of zirconia. The only recognized glasses showing zirconia crystals are SG, SE, and SN even at heating temperatures ranging from 650 to 710 °C. The glasses SG and SE showed a diffraction peak at $2 = 21.2$ at 730 C, this could be traced to plane orientation (111) of low-carnegieite. The Two additional peaks obtained from diffractometer angles on nepheline ($NaAlSiO_4$, hexagonal) developed at $2\theta = 23.2°$ and 27.3°, which were ascribed to the planes orientation (201) and (210), respectively, increased the heating temperature from 750 to 780 C. Increasing in the temperature of glasses to 750 °C the glass SN, begin transformation at low-carnegieite crystalline phase, even the same temperature was observed on the weak diffraction peaks from nepheline [129]. We also observed evidence of low intensity and a broadening shape from the X-ray diffractometer angle of glass SN. The low crystallinity was noticed in the entire matric. Fig. 8, shown below also displayed clearly the transmittance curves of the glass SG, SE, and SN heat treated at 650–780 °C for 5 h. At high temperature of over 730 °C, both glasses lost a substantial amount of transparency in Fig. 1. Even at a heating temperature of 780 °C, the transparent ceramic SN glasses maintained a reasonable amount of 60% limpidity at noticeable wavelengths [129] (see Fig. 15) (see Fig. 14).

At 750 °C we observed that the X-ray diffractometer patterns of crystallized glasses for 1 h, 3 h, 5 h, and 7 h are presented in Fig. 13. In all the three glasses, we noticed the presence of phases in zirconia, low-carnegieite, and nepheline crystalline glass and discovered that they all fall in order as the exposure time increases from 1 to 7 h. There is also evidence of varying diffraction peaks from nepheline crystals shown in the x-ray diffractometer patterns in glasses with SG after 3 h of heating, but not in glass SN and SE after more than 5 h.

5.4. *Transparent ferroelectric ceramics materials*

Transparent ferroelectric ceramics (TFC) are potential material for optoelectronic devices because of the coefficient of electro-optic device, infrared ray within the range of 0.37–6.5 bm and extremely high optical transmittance in a visible form. This is unlike monolithic crystals that is clearly administered by symmetry, polarization is the major determinant of the optical axis in TFC, and its orientation and optical features are susceptible to changes by a specific action caused by tension. This is clearly known illumination, thermal field, and irradiation) [3]. It is feasible to flip tiny local regions without changing polarization in nearby areas due to phases purity and the morphological structures. The diffusion of the phase transition (PT) in TFC is easily detected, and the coefficient of electrooptic coefficients gives room for a wider temperature range for ease operation. In terms of promising uses, TFC are seen as the major link that distinguishes the liquid crystals, laser diodes, electroluminescent layers from others, the reason for this performance could be attributed to the TFC operational speed, many colors are advantageous in operational speed, a wider viewing angle and multi-color capability, in higher environmental and irradiation resistance; one of the drawbacks is that it is very expensive in terms of operating voltage, uneasy to insert in an integrated method and electrooptic single crystals compared to TFC in which the there

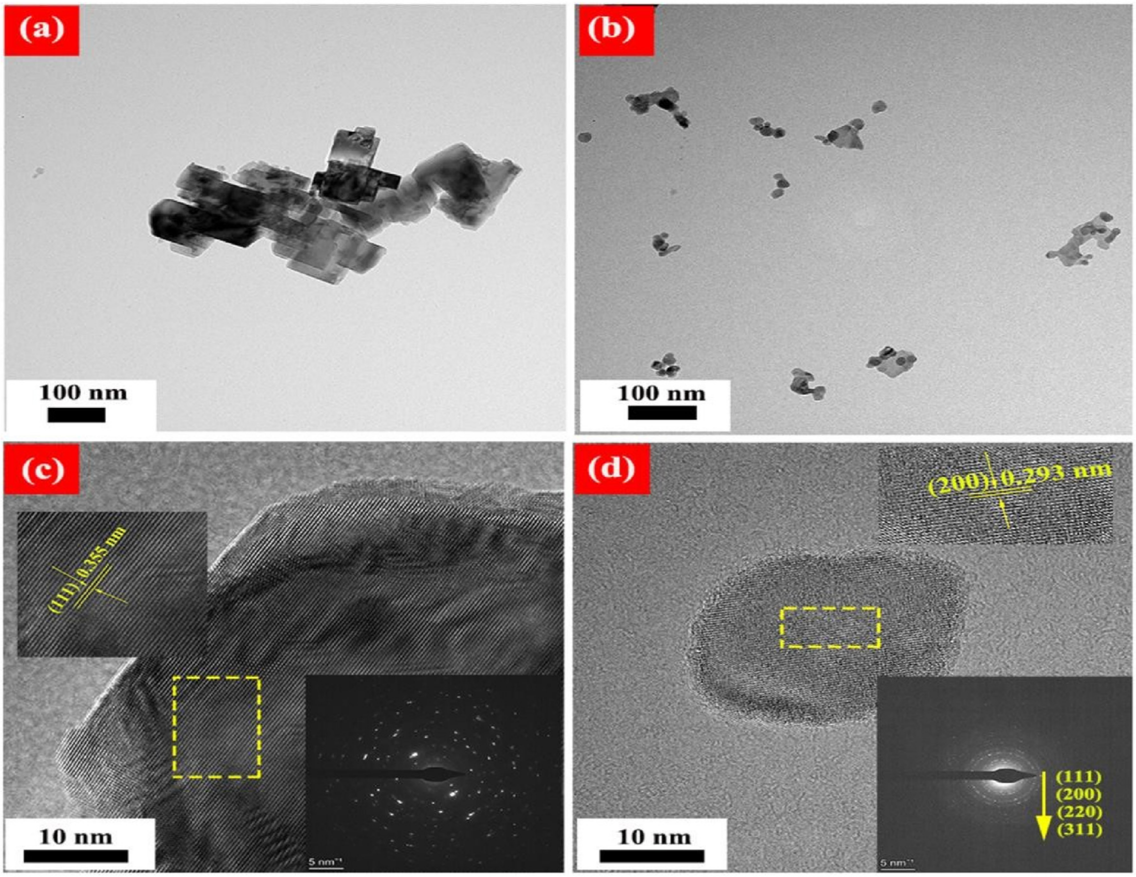

Fig. 12 – TEM images of Pr^{3+}- doped as-synthesized BaF2 nanopowders at 0.1 at percent (a) and 5.0 at percent (b); (c) and (d) are HRTEM images of comparable particles in (a) and (b), correspondingly. The appropriately chosen region electron diffraction pattern is shown in the insert [127,128].

are varying compositions that gives room for variable compositional changes, this permit a widespread viewing angle and multi-color capability Ferroelectric thin films are promising in based on functional integrated optoelectronic structures [130]. Integrating enriched Polycrystalline crystalline with the main chemical composition of the ferroelectric materials, the Pb0.97Bi0.02(Zr0.51Ti0.49)0.98(Nb2/3Mn1/3) 0.02O3 (P) and ferrite powder with the chemical formula Ni0.5Zn0.5Fe2O4 resulted in ferroelectric–ferromagnetic ceramic composites.

6. Mullite

A lot of interest has recently been channeled towards an effective utilization of lightweight thermal insulating materials as a noteworthy energy materials for their uses in so many metallurgical industries including the energy storage and oil (gas) transport system [131,132]. Lightweight thermal insulating materials such as mullite, particularly in the energy storage industry, can easily reduce energy usage. As a result,

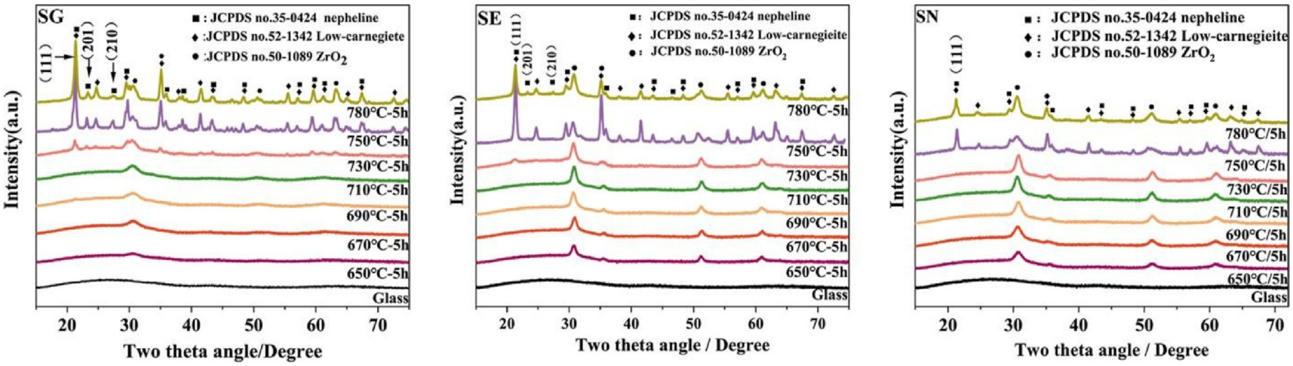

Fig. 13 – XRD patterns of the glasses heat treated at 650–780 °C for 5h [129].

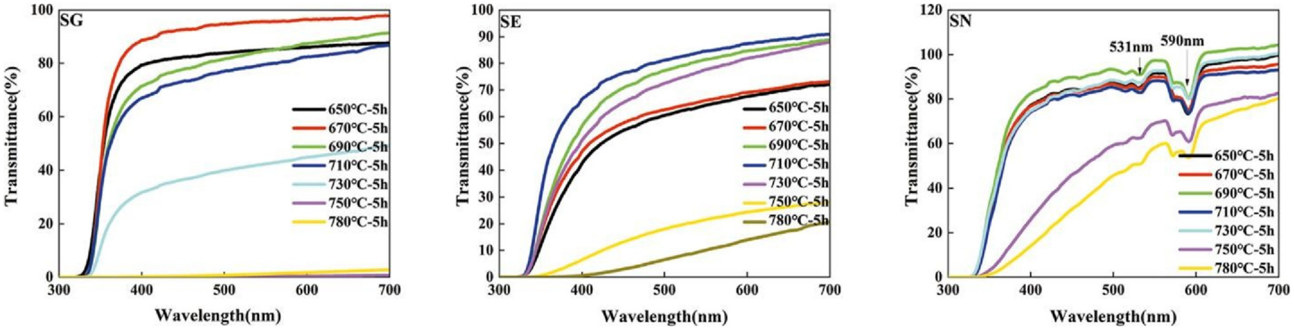

Fig. 14 – Transmittance curves of the glasses heat treated at 650–780 °C for 5 h [129].

it's critical to develop improved techniques and even some materials needed to produce this ceramic with high-performance thermal insulating properties. One of the researched areas to figure out a solution is by considering lightweight porous mullite ceramics that have properties such as (low thermal conductivity, acid-alkali corrosion resistance, and compressive strength) [133–135]. Since the 1990s, significant work has been invested into creating novel pore configurations to enhance the performance of porous mullite ceramics, including the application of materials that tends to create pore-forming properties [136,137], such as sol–gel vacuum impregnation [138], and foam-gel-casting [139,140]. Regrettably, all the processes have varying drawbacks, such as gradual reduction in the purity level of mullite materials with high porosity as chemicals were added to synthesis byproducts that impair the environment, the processing techniques of achieving this thermal insulating materials is quite challenging and manufacturing cost is expensive. Mullite ceramics' optical transparency, along with their superior thermal-shock resistance and high-temperature strength, makes them ideal for use as an optical window material at high temperatures.' New study conducted concentrating on absorption spectrum performance inside the mid-infrared portion of the electromagnetic spectrum has revealed that mullite's photon energy capabilities positively relate with those of other promising materials including mica schist and diamond.

6.1. *Morphological and spectroscopic analysis of mullite ceramic materials*

Fig. 17 reveals the energy dispersive spectroscopy analysis on the distribution of elemental compositions of the sintered sample. Aluminum, Silicon, and Oxygen were dispersed in the sintered samples, as shown in EDS analysis of Fig. 13a and b. The sintered samples only included mullite phase, as a result, the technology might be able to guarantee the purity of mullite fibrous ceramics.

7. Lighting applications of transparent yttria stabilized zirconia (YSZ) ceramics

Transparent ceramics has some significant functions and combination of properties due to their high thermomechanical properties, they penetrate deeper into the ultraviolet and infrared light more than the ceramic glasses and polymers on displaying qualities which include lasing, electronic conduction, magnetooptic together with electrooptic and ferroelectricity activity. The production patterns are into near-net forms at a cheaper rate than single crystals, and their characteristics can be modified by altering their microstructures by the introduction of dopants and secondary phases [142]. Following a thorough discussion, it will be clear that transparent ceramics are excellent for a variety of applications,

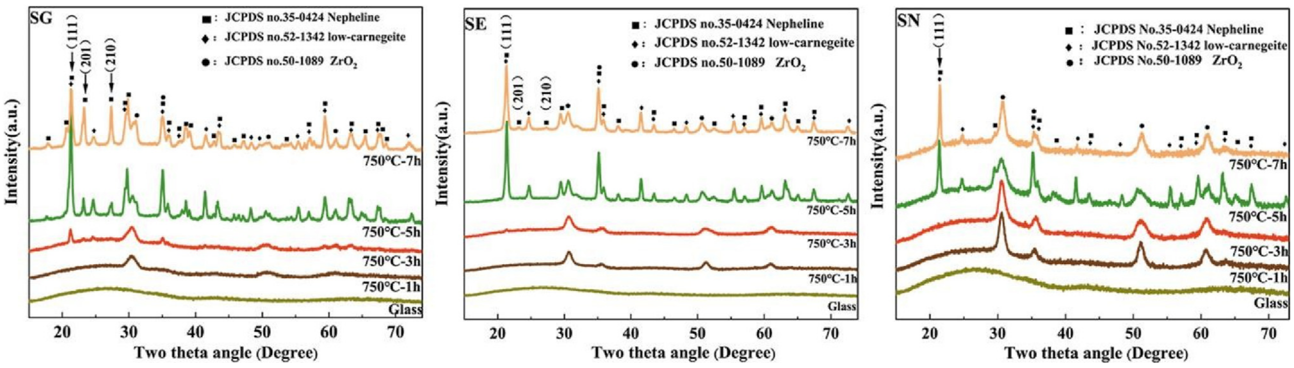

Fig. 15 – XRD patterns of the glasses heat treated at 750 °C for 1–7 h [129].

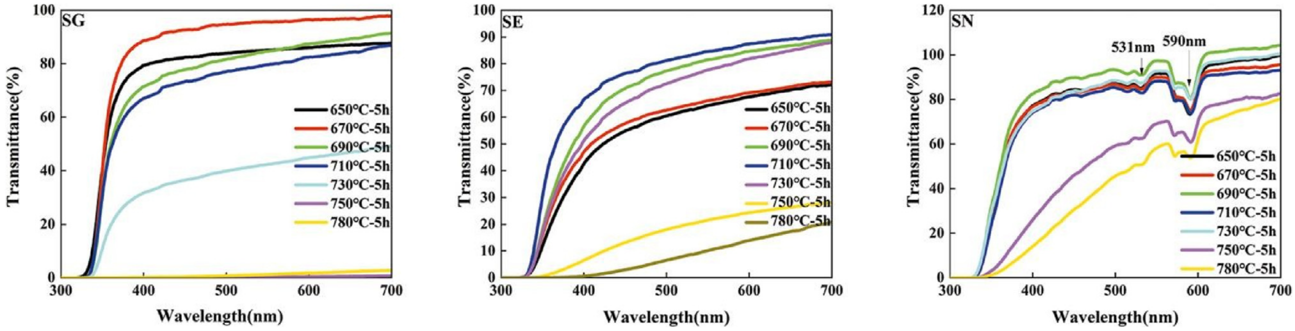

Fig. 16 – Shows some evidence of some transmittance curves for glasses heat-treated at 750 °C for 1–7 h [129] For transparent ceramics materials, the difference between "in-line" and "real in-line" transmittance measurements for transparent ceramics materials are shown below.

including lasers, armors, and lightning, thanks to their unique optical transparency and the general properties of ceramics. Some of the application areas are further discussed below:

(i) Transparent ceramic for Laser application

Due to the numerous benefits of ceramics over single crystals, it has gained a widespread attention in ceramic laser technology. Ceramics are suitable for high power laser production because they can be fabricated in large quantities. Also, they can be used to create composite laser media with intricate structures that would be challenging to create with single crystals, as well as a gain medium for fiber lasers with good beam quality. Furthermore, in comparison with single crystals, transparent ceramics can be uniformly and strongly doped with laser-active ions. All these has tremendously increased the use of transparent ceramics in the production of lasers with tailored specific functions at low cost for commercial usage [3].

(ii) Transparent ceramic for Armor application

Transparent armor is frequently used as ballistic helmets and visors for personnel protection, as windows for armored cars and ground vehicles, and as windshields and lookdown windows for aircraft. For the requisite multi-hit ballistic protection, the commonly employed glass-based transparent armor windows are often more than five inches thick. The comparatively delicate glass front can be damaged by rocks and blowing sand in the field, increasing replacement costs in addition to increasing wear costs for tactical vehicles that are already pushing their weight limits. As a result, it is imperative to decrease the weight of transparent armor systems while enhancing their ballistic protective qualities. For multimode weapon systems exposed to adverse weather conditions, there is also a requirement for wide windows and domes. Choices are frequently constrained to a small number of materials when both strength and hardness are important performance parameters. These are the single crystals of

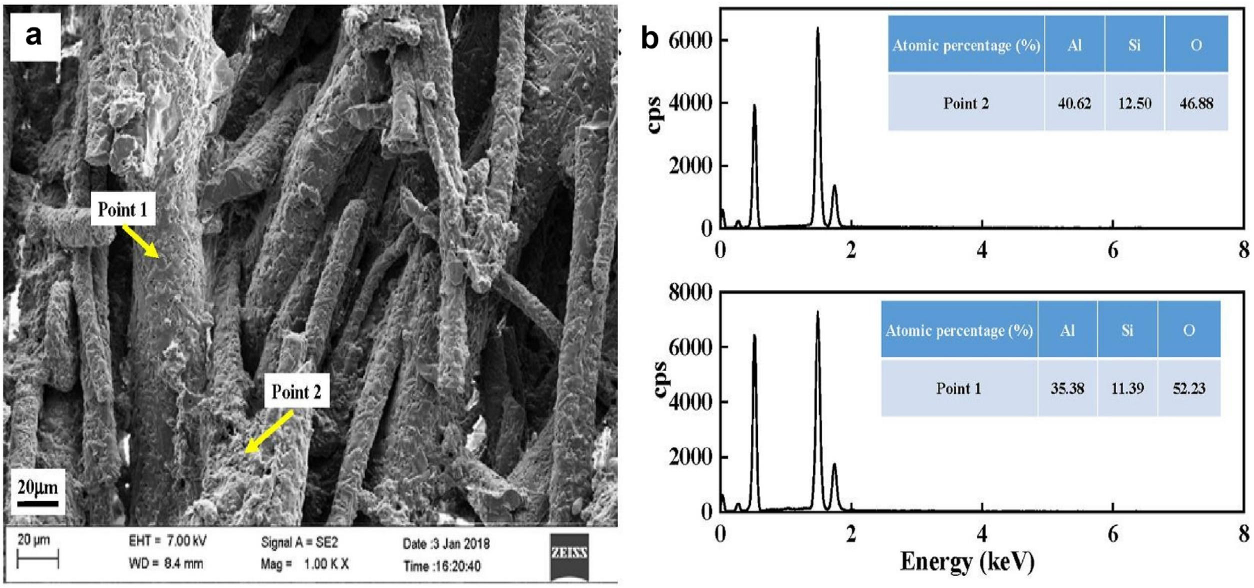

Atomic percentage (%)	Al	Si	O
Point 2	40.62	12.50	46.88

Atomic percentage (%)	Al	Si	O
Point 1	35.38	11.39	52.23

Fig. 17 – Morphological structure (a) and Energy dispersive spectroscopy (b) analysis of ceramic fibrous mullite [141].

spinel (magnesium aluminate), sapphire (aluminum oxynitride), and oxynitride (sapphire) [143,144]. These three materials have long been thought of as potential substitutes for ballistic glasses in transparent armor applications due to their exceptional strength and hardness.

(iii) Transparent ceramic for lighting application

For focused-beam, short-arc lamps with a variety of fillers working at temperatures higher than the melting point of quartz, transparent ceramic materials with suitable thermal and mechanical qualities are particularly helpful. For many years, discharge lamps' envelopes have been made of coarse-grained transparent polycrystalline alumina ceramics (PAC). The lighting sector has benefited from the transparent polycrystalline alumina (PCA) doped with additives derived from magnesia, which was first identified in the 1960s. High-pressure sodium lights were made and widely used thanks to it [145]. Due to the regular transparent alumina's inherent translucency, metal halide lamps with round [146] or cylindrical [146,147] translucent alumina tubes were first produced for general illumination applications in the 1990s. The 1994 introduction of metal halide lamps by Philips resulted in a better "white" light. Al_2O_3 is practically unreplaceable as an envelope of exceptional chemical resistance in these lamps because they operate at temperatures about 1200 °C [148,149].

7.1. Transmission, transmittance, transparency and translucency properties of transparent ceramic materials

It is essential for the transmission of radiation from electromagnetic properties of a specific rate or rate range a solid plate (slab) to be transparent. This is commonly referred to as transmission. Although transparency can include different waves from radio, microwaves, thermal radiation, X-rays, and gamma rays, we will focus on visible light and its immediate neighbours in this work (UV and near-IR). The term "transmittance" should be used to describe the quantitative measure of transmission (even though researchers from different countries prefer to apply the two terms simultaneously). Absorption can reduce the level of transmittance of a signal. Where λ is the wavelength and n (1) is the number of occurrence of the cubic crystallite materials in Fig. 18, Tmax show the maximum number of transmittance in Fig. 19. When there is no absorption, the transmittance is at its highest. Because some incident light can be diverted or "dissipated" into other directions even if it is not absorbed, the transmittance at high frequency is required, not necessarily a prerequisite for transparency.

Rather than being transparent in nature, the output of the experiment may end up opaque, as a result, whole onward transmittance (quantifying light transmitted in all directions up to 90° from the incoming light direction), forward transmittance (encompassing directions up to a defined angle of 90°), and in-line transmittance (encompassing directions up to a defined angle of 90°) can be distinguished in Figs. 18 and 19. Meanwhile the flawless in-line transmittance can sometimes remain accurately measured (due to the spectrometer's restricted aperture width required to achieve non-zero light intensity on the detector), low-angle forward transmittances must be used to extrapolate it to 0. An applied approach simply measures transmittance with a tiny aperture, such as one traditionally configured to be the one with the smallest aperture 0.5 half-angle. All of that is referred to as "real" in-line transmittance, or RIT [152]. The concept of "genuine" in-line transmittance, on the other hand, is clearly a practical custom with no physical basis. The optimum in-line transmittance (not for 0.5) is the one projected for 0 regardless, and the 0.5 transmittance is not any more or no worse "authentic" than almost any low-angle advance transmittance. Even though it is essential to estimate angles of transmittance for angles spanning as of 0–0.5 using angular dependence of scattering, this is rarely performed so many materials containing ceramics research. As a result, rather than determining the theoretical (0) in-line transmittance, the study compares that to the actual (0.5) in-line transmittance (whether they have a spectrophotometer set up for such measurements) or another estimated number [152].

Spectrophotometer light detectors typically collect light at angles of up to 3–5° [153], as shown in Fig. 20. A sharp noticeable mixture was observed when scattering in the system, was detected and capture alongside with the "unscattered" light (or, simply put the diversion of light was found tending towards the incident light ways), resulting in ostensibly generating transmittance at elevated levels, the same scenario was observed in the translucent glass rather than transparent. As a result, for these types of studies (where experimental findings are compared to theoretical expectations), it's critical to maintain the spectrophotometer aperture as tiny as feasible (due to the required amount of intensity needed for a dependable sensor reaction which is otherwise known as a detector). Based on this, the main distinguishing factors for "in-line transmittance" and "true in-line transmittance" have been made. Manufacturers of ceramic discharge lamps coined the term "real in-line transmittance" (RIT) to provide a legitimate conditions required for transparency come to be [153], this can as well be described in the form of overall transmittance taken at an aperture half-angle of 0.5, as shown in Fig. 16. Attempt was made to select 0.5 as the permissible angle needed for concession between being narrow enough to limit the influence of scattered light while yet being big adequate for useful quantity [153]. According to Wang et al. [154], he newly proved in his research that a translucent sample's normal (3–5) in-line transmittance can be equivalent to that of a plainly transparent one, although the RIT reveals a distinct difference between the two (with the RIT being lower). Furthermore, the difference between the "in-line" and "actual in-line" transmittance for the translucent sample was striking, but the difference between the "in-line" and "real in-line" transmittance for the obviously transparent samples was small. This demonstrates that, in the case of transparent materials, not only light scattering but also measurement circumstances have a significant impact on the observed transparency [154].

8. Transparent ceramic materials in biomedical applications

Because standard bioceramic materials are opaque, it is impossible to observe cells directly in transmission mode

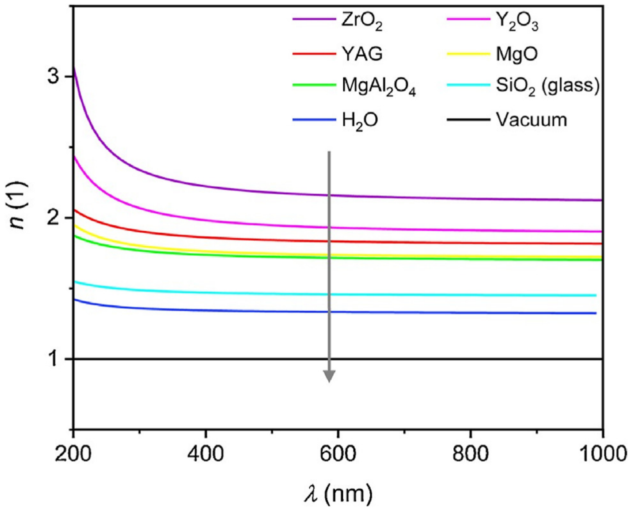

Fig. 18 – Wavelength dependency of the refractive index for vacuum [70], amorphous silica (silica glass) [71], and cubic crystallites of chosen transparent ceramics [72,150].

using a light microscope. Because the optical transparency of transparent hydroxyapatite (tHA) ceramics allowed them to detect cellular activities under transmitted light, John et al. investigation was used them to straightly monitor some cell in the body and conduct time-lapse investigations [155]. Transmission light microscopy was employed to develop rat calvaria osteoblasts (RCO) on the transparent tHA ceramics, demonstrating the bioceramic materials' high cytocompatibility. Improved aqueous phosphate (ALP) activation suggested osteoinductive hBMSC transformation into the osteoblastic lineage, confirming favourable proliferation. Furthermore, on the tHA samples, human monocytes were distinguished from osteoclast-like cells, which was validated by fluorescence transparent ceramics materials containing multi-nucleated cells. Multinucleated cells on transparent ceramics were imaged using microscopy Bodhak et al. [156]. Considering the biological presentations of profitable $MgAl_2O_4$ also AlON® transparent ceramic materials, the transparent ceramics exhibit no toxicity. According to the $MgAl_2O_4$ and AlON, transparent ceramics were better than commercially obtained titanium products. In terms of cell interaction and mechanical properties behaviour, $MgAl_2O_4$ ceramics outperformed AlON ceramics. Cosmetic orthodontic brackets made of transparent MgAl2O4 ceramics have recently been tested [157]. The biomaterial-oral mucosa interaction is a typical way to assess the candidature biocompatibility for dental claims. This is a clear indication of the good biocompatibility nature of transparent MgAl2O4 materials in the health sector.

Furthermore, the $MgAl_2O_4$ ceramic possesses a very active mechanical/optical and physico-chemical performance needed for orthodontic brackets subjected to thermal stress, resistance to corrosion, and biological attack vivo [158]. However, the use of transparent ceramics in the biological sector is still in its early stages, necessitating additional research.

From the image in Fig. 21, the labelled (A) is representing the craniectomy over right back of the brain with unprotected Subarachnoid Space (B) mean the WttB implant stability inside craniectomy and fixation to skull with dental cement, (C) WttB implant placement within craniectomy and fixation to skull with dental cement (D) WttB implant placement within craniectomy and fixation to skull with dental cement, (E) WttB implant placement within cr Illustrations of a laser speckle image acquisition. Surgical and imaging procedures for the n = 5 mice over time. sld stands for super-luminescent diodes; pc stands for polarization controller; c stands for collimator; pbs stands for polarization beam splitter; pm stands for polarization modulator; bs stands for beam splitter; ndf stands for neutral density filter; lsc stands for line scanning camera.

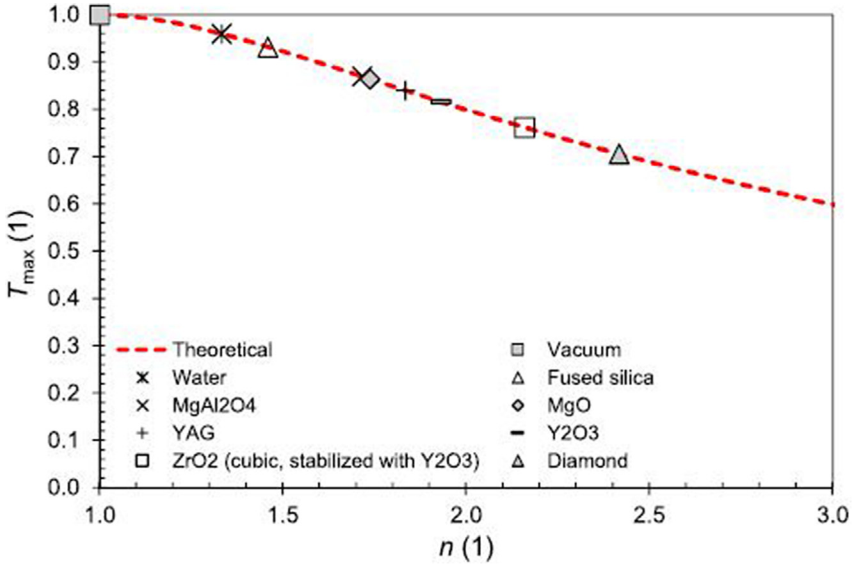

Fig. 19 – Wavelength of 589 nm, based on several cubic crystal structures for transmittance on refractive index in Vacuum, water, amorphous silica, and diamond [151].

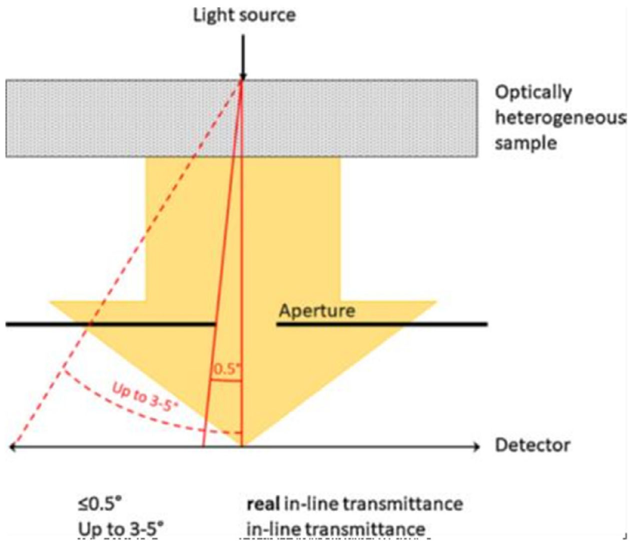

Fig. 20 – Illustration of dissimilarity amid "in-line" in addition to "real in-line" transmittance measurements [151].

Many neurological illnesses, such as cerebral oedema, stroke, and cancer, have shown potential in using laser-based approaches to improve diagnosis and therapy [89]. Nevertheless, invasive craniotomies are frequently required to enable optical access to the brain because the cranial bone's limited transparency to therapeutically important laser wavelengths (i.e. 550-1300 nm). It limits the approaches' eventual value, especially in applications that require chronically repeating access over broad areas. Some new studies [83,91] have shown that flattening the skull can increase cranial transparency. However, because this reduces brain protection, accompanying safety issues may prevent such procedures from being translated to the clinic. In other experiments, clear the cranium six has been replaced with glass-based implants, and thinned-skull preparations have been strengthened with glass-based implants. On the other hand, ordinary glasses have a very low fracture toughness (KIC = 0.7–0.9 MPa m1/2), raising the risk of catastrophic fracture limiting the usage of such implants outside of the laboratory. As a result, the search for alternative materials that are more suitable for therapeutic purposes is fuelled.

Fig. 22(b–d) illustrates the right-sided craniectomies carried out on sedated mice followed by dental cement attachment on the animal with nc-YSZ implants. The early viability of the nc-YSZ implant was assessed using optical coherence tomography OCT, a common optical imaging technique. Imaging was done across a 22 mm^2 region on the position that suits the implant, preferably in coronal direction for both the nc-YSZ implant and the normal skull.

9. Summary of findings and recommendations for future prospects

1. From literature, we discovered that solid-state lasers were used for the production of most transparent ceramics materials. Among the numerous application areas, studies have shown that transparent ceramic materials can used in scintillation, illumination, military armors known as

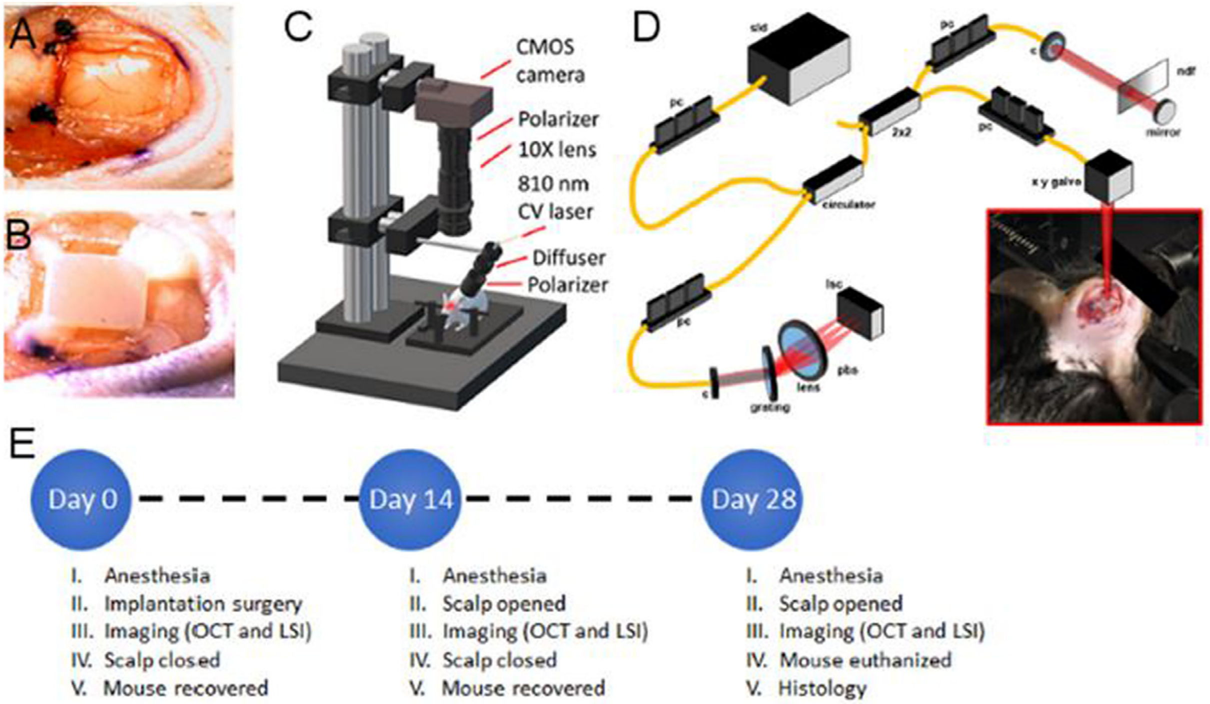

Fig. 21 – Transparent nanocrystalline Yttria-stabilized –zirconia used for chronic brain imaging primarily for Cranial Implant (reproduced with permission from [89].

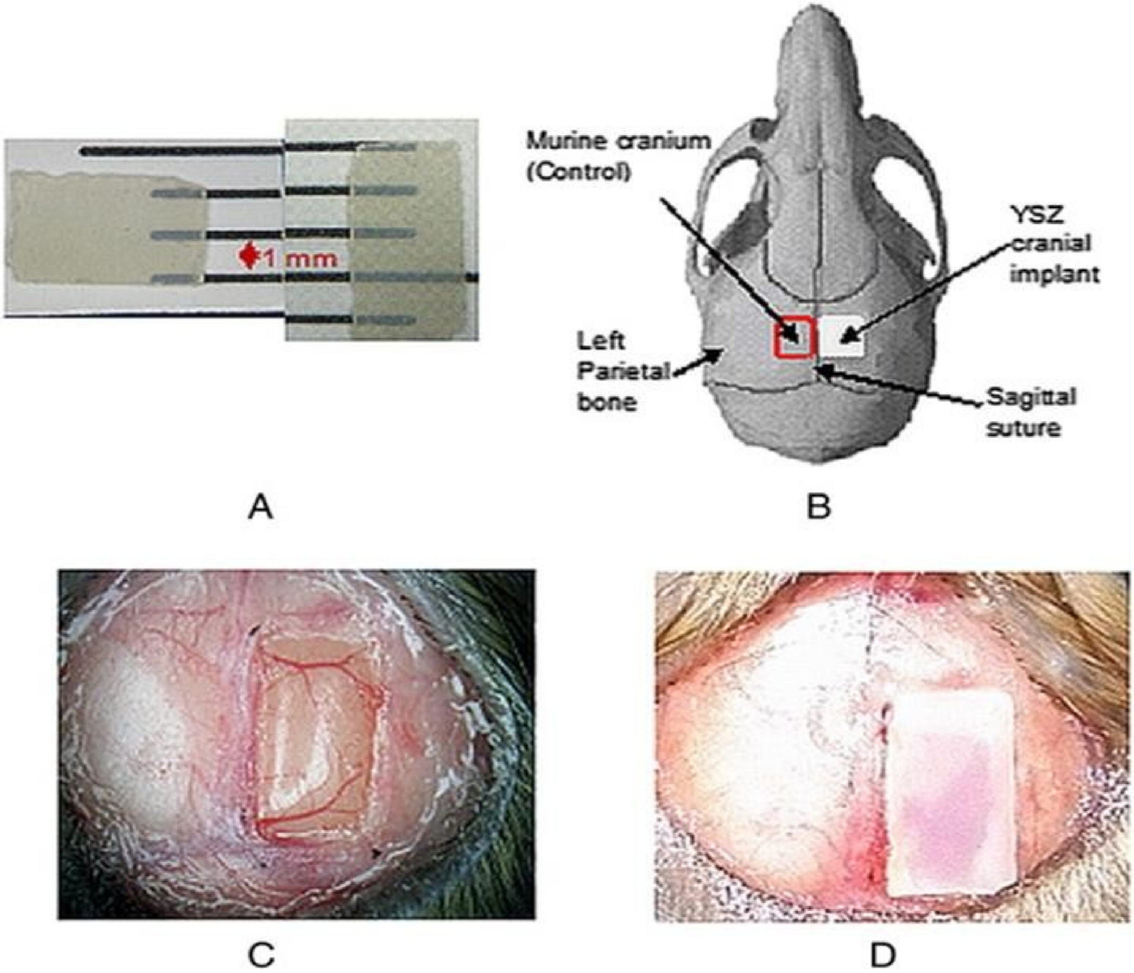

Fig. 22 – Nc-YSZ transparent cranial transplants showing: (A) transplant on a coloured image scale to establish limpidity; (B) craniotomy position on a mouse skull; (C) a photo of a craniectomy and the duramater undamaged; besides (D) a photo after implantation location [89].

transparent ceramic armors, scanning electron microscope lenses, materials for biomedical purposes, and electro-optical devices. Furthermore, LEDs and LDs with high performance levels are expected to become the primary lighting sources in both household and industrial settings. The fundamental requirement for this application is from doped transparent ceramics materials with bright features. In addition, the replacement of screens for smartphone glasses could be easily achieved through the applications of low-cost, transparent ceramics with high mechanical properties, which is significant considering how important smartphones are in our everyday lives.

2. From various investigations on transparent ceramics, we discovered that transparent ceramic materials have better performance than ordinary glass ceramic and polymers in all applications in terms of optical, mechanical and thermal stability properties, permitting their application in high temperature areas and in more demanding areas environments. Transparent ceramics are also useful scintillators. It has been discovered that the transparent armors manufactured with ceramic materials stand to provide better and suited performance because they are substantially thinner and lighter than the ones produced with other materials. Nonetheless, transparent ceramics applications outside of solid-state lasers are in their developmental stage, suggesting there are numerous prospects trending in these domains and that have further potential claims will be studied in the future. As a result, transparent ceramic research in materials science and engineering is projected to have a promising future.
3. This study can confidently ascertain that transparent ceramics are a novel class of resources met to be exploited in high-temperature technology applications. To meet the demands of many prospective applications, several processing procedures have been devised to generate translucent ceramics with an extensive variety of structures and qualities. To begin with, not all materials are suitable for making transparent ceramics. A highly symmetric crystallographic features such as hexagonal closed pack, tetragonal crystal structures and cubic, meet the fundamental criteria of transparency.

4. Finally, a good description of the production process for transparent ceramic materials must be described and scrutinized. The concentration of Y2O3 powder in slurry during preparation, for example, might have a significant impact on the overall ceramic and its optical properties; however, variations seen in characteristics of as-received materials and their slurries form with varied compacted compositions are yet to be determined. It is an indication that the optical qualities of ceramics are more affected by their microstructure than other engineering properties. As a result, more research into the link between morphological structures, control constraints, and optical transparency is needed. In addition to that purpose, innovative methodologies plus approaches for characterizing transparent ceramics with comparable morphological structures but varying optical transparencies should be developed.
5. Previous research has revealed the application of vacuum sintering to synthesise transparent ceramic materials at high temperatures. Transparent ceramics may also be produced using some other powder metallurgical techniques, on the other hand, necessitates a costly production process. In contrast, hot pressing as one of the powder metallurgy techniques has contamination problem due to direct contact of the graphite die with sintered compacts. As a result, the diffusion of carbon into the sintered compacts is unavoidable irrespective of the sintering temperature used. A novel spark plasma sintering process will be of great benefit in the production of ceramic, which necessitate the concept of this review article.

Declaration of Competing Interest

The authors declare that they have no known competing financial interests or personal relationships that could have appeared to influence the work reported in this paper.

Acknowledgment

The authors would like to extend his appreciation to Deanship of Scientific Research at King Khalid University in Saudi Arabia for funding this work through the research group program under grant No. RGP.2/12/43. The authors also expressed gratitude for the funds provided by the University Research Committee (URC) and also the assistance provided by the University of Johannesburg's center for Nanomechanics and Tribocorrosion in establishing an appropriate research environment. Our research lab colleagues and staff from the Engineering Materials Development Institute EMDI, Akure were very helpful.

REFERENCES

[1] Xiao Z, Yu S, Li Y, Ruan S, Kong LB, Huang Q, et al. Materials development and potential applications of transparent ceramics: a review. Mater Sci Eng R Rep 2020;139:100518.
[2] Al Saghir K, Chenu S, Veron E, Fayon F, Suchomel M, Genevois C, et al. Transparency through structural disorder: a new concept for innovative transparent ceramics. Chem Mater 2015;27:508–14.
[3] Wang S, Zhang J, Luo D, Gu F, Tang D, Dong Z, et al. Transparent ceramics: processing, materials and applications. Prog Solid State Chem 2013;41:20–54.
[4] Kawajiri K, Tahara K, Uemiya S. Lifecycle assessment of critical material substitution: indium tin oxide and aluminum zinc oxide in transparent electrodes. Resources, Environment and Sustainability 2022;7:100047.
[5] Kong LB, Huang Y, Que W, Zhang T, Li S, Zhang J, et al. Transparent ceramic materials. In: Transparent ceramics. Springer; 2015. p. 29–91.
[6] Petrunin V, Korovin S. Preparation of nanocrystalline powders of ZrO2, stabilized by Y2O3 dobs for ceramics. Phys Procedia 2015;72:544–7.
[7] Wang J, Zhang F, Chen F, Zhang J, Zhang H, Tian R, et al. Effect of Y_2O_3 and La_2O_3 on the sinterability of γ-AlON transparent ceramics. J Eur Ceram Soc 2015;35:23–8.
[8] Vahldiek F. Translucent ZrO_2 prepared at high pressures. J Less Common Met 1967;13:530–40.
[9] Chevalier J, Deville S, Münch E, Jullian R, Lair F. Critical effect of cubic phase on aging in 3 mol% yttria-stabilized zirconia ceramics for hip replacement prosthesis. Biomaterials 2004;25:5539–45.
[10] Liu Q, Jing Y, Su S, Li X, Liu X, Feng Y, et al. Microstructure and properties of $MgAl_2O_4$ transparent ceramics fabricated by hot isostatic pressing. Opt Mater 2020;104:109938.
[11] Paygin V, Stepanov S, Dvilis E, Khasanov O, Alishin T, Valiev D. Effect of technological parameters on optical and mechanical properties of Spark Plasma Sintered transparent YSZ ceramics. Ceram Int 2021;47:11169–75.
[12] Lei L, Fu Z, Wang H, Lee SW, Niihara K. Transparent yttria stabilized zirconia from glycine-nitrate process by spark plasma sintering. Ceram Int 2012;38:23–8.
[13] Zeng W, Gan X, Li Z, Zhou K. Effect of TiC addition on the microstructure and mechanical properties of TiN-based cermets. Ceram Int 2017;43:1092–7.
[14] Peuchert U, Okano Y, Menke Y, Reichel S, Ikesue A. Transparent cubic-ZrO2 ceramics for application as optical lenses. J Eur Ceram Soc 2009;29:283–91.
[15] Alaniz J, Perez-Gutierrez F, Aguilar G, Garay J. Optical properties of transparent nanocrystalline yttria stabilized zirconia. Opt Mater 2009;32:62–8.
[16] Dash A, Kim B-N, Klimke J, Vleugels J. Transparent tetragonal-cubic zirconia composite ceramics densified by spark plasma sintering and hot isostatic pressing. J Eur Ceram Soc 2019;39:1428–35.
[17] Anselmi-Tamburini U, Woolman JN, Munir ZA. Transparent nanometric cubic and tetragonal zirconia obtained by high-pressure pulsed electric current sintering. Adv Funct Mater 2007;17:3267–73.
[18] Tsukuma K, Yamashita I, Kusunose T. Transparent 8 mol% Y_2O_3–ZrO2 (8Y) ceramics. J Am Ceram Soc 2008;91:813–8.
[19] Zhang H, Kim B-N, Morita K, Hiraga HYK, Sakka Y. Effect of sintering temperature on optical properties and microstructure of translucent zirconia prepared by high-pressure spark plasma sintering. Sci Technol Adv Mater 2011;12(5). https://doi.org/10.1088/1468-6996/12/5/055003.
[20] Bertrand A, Carreaud J, Delaizir G, Duclère JR, Colas M, Cornette J, et al. A comprehensive study of the carbon contamination in tellurite glasses and glass-ceramics sintered by spark plasma sintering (SPS). J Am Ceram Soc 2014;97:163–72.
[21] 藤原巧 本間剛, 高橋儀宏 紅野安彦, 小松高行. レーザー学会研究会報告= reports on the topical meeting of the laser society of Japan 303, 27-31, 2002-11-01. J Non-Cryst Solids 1995;189:16.

[22] Singarapu B, Galusek D, Durán A, Pascual MJ. Glass-ceramics processed by spark plasma sintering (SPS) for optical applications. Appl Sci 2020;10:2791.

[23] Goutaland F, Mortier M, Capoen B, Turrell S, Bouazaoui M, Boukenter A, et al. UV-assisted crystallisation of tellurite and germanate-based glasses. Opt Mater 2006;28:1276–9.

[24] Chavan S, Pillai K, Tyagi A. Combustion synthesis of nanocrystalline yttria: tailoring of powder properties. Mater Sci Eng, B 2006;132:266–71.

[25] Benitez T, Gomez SY, de Oliveira APN, Travitzky N, Hotza D. Transparent ceramic and glass-ceramic materials for armor applications. Ceram Int 2017;43:13031–46.

[26] Thomas J, Kumar HP, Pazhani R, Solomon S, Jose R, Koshy J. Synthesis of strontium zirconate as nanocrystals through a single step combustion process. Mater Lett 2007;61:1592–5.

[27] Yoshida H, Morita K, Kim BN, Hiraga K, Yamanaka K, Soga K, et al. Low-temperature spark plasma sintering of yttria ceramics with ultrafine grain size. J Am Ceram Soc 2011;94:3301–7.

[28] Gong H, Tang D-Y, Huang H, Zhang T-S, Ma J. Effect of grain size on the sinterability of yttria nanopowders synthesized by carbonate-precipitation process. Mater Chem Phys 2008;112:423–6.

[29] An L, Ito A, Goto T. Transparent yttria produced by spark plasma sintering at moderate temperature and pressure profiles. J Eur Ceram Soc 2012;32:1035–40.

[30] Luo J, Zhong Z, Xu J. Yttrium oxide transparent ceramics by low-temperature microwave sintering. Mater Res Bull 2012;47:4283–5.

[31] Mouzon J, Maitre A, Frisk L, Lehto N, Odén M. Fabrication of transparent yttria by HIP and the glass-encapsulation method. J Eur Ceram Soc 2009;29:311–6.

[32] Jose SM, Mathew C, Thomas JK. Fabrication of Dysprosium doped Y2O3 infrared transparent ceramic materials by a microwave sintering technique. Mater Today Proc 2020;24:2383–93.

[33] Huang Y, Jiang D, Zhang J, Lin Q. Precipitation synthesis and sintering of lanthanum doped yttria transparent ceramics. Opt Mater 2009;31:1448–53.

[34] Dasgupta N, Krishnamoorthy R, Jacob KT. Glycol–nitrate combustion synthesis of fine sinter-active yttria. Int J Inorg Mater 2001;3:143–9.

[35] Kong LB, Huang Y, Que W, Zhang T, Li S, Zhang J, et al. Sintering and densification of transparent ceramics. In: Transparent ceramics. Springer; 2015. p. 467–517.

[36] Luo W, Xie R, Ivanov M, Pan Y, Kou H, Li J. Effects of LiF on the microstructure and optical properties of hot-pressed MgAl2O4 ceramics. Ceram Int 2017;43:6891–7.

[37] Ikesue A, Aung YL. Ceramic laser materials. Nat Photonics 2008;2:721–7.

[38] Viter R, Iatsunskyi I. Metal oxide nanostructures in sensing. In: Nanomaterials design for sensing applications. Elsevier; 2019. p. 41–91.

[39] Pan Z, Wang Y, Huang H, Ling Z, Dai Y, Ke S. Recent development on preparation of ceramic inks in ink-jet printing. Ceram Int 2015;41:12515–28.

[40] Wang Y, Yu S, Chu J, Chen D, Chen J. Study on the copper and iron coexisted coloring glaze and the mechanism of the flambe. J Eur Ceram Soc 2018;38:3681–8.

[41] Opuchovic O, Kareiva A. Historical hematite pigment: synthesis by an aqueous sol–gel method, characterization and application for the colouration of ceramic glazes. Ceram Int 2015;41:4504–13.

[42] Akinribide O, Obadele B, Akinwamide S, Bilal H, Ajibola O, Ayeleru O, et al. Sintering of binderless TiN and TiCN-based cermet for toughness applications: processing techniques and mechanical properties: a review. Ceram Int 2019;45:21077–90.

[43] Coffey N. The effects of colorant oxides and firing rate on the nucleation and growth of zinc silicate crystals in crystalline glazes. 2011.

[44] Wannagon A, Prasanphan S, Sanguanpak S. Characterization of Li–Zn–Fe crystalline phases in low temperature ceramic glaze. J Eur Ceram Soc 2013;33:653–60.

[45] Viswanath N, Grandhi GK, Kim HJ, Zhuang Y, Xie R-J, Im WB. A new persistent blue-emitting phosphor: tailoring the trap density for enhancing the persistent time. Appl Mater Today 2020;18:100518.

[46] Li H, Pang R, Luo Y, Wu H, Zhang S, Jiang L, et al. Commendable Pr 3+-activated Ba 2 Ga 2 GeO 7 phosphor with high-brightness white long-persistent luminescence. J Mater Chem C 2019;7:6698–705.

[47] Wang B, Li X, Chen Y, Chen Y, Zhou J, Zeng Q. Long persistent and photo-stimulated luminescence in Pr3+-doped layered perovskite phosphor for optical data storage. J Am Ceram Soc 2018;101:4598–607.

[48] Wang C, Jin Y, Lv Y, Ju G, Liu D, Chen L, et al. Trap distribution tailoring guided design of super-long-persistent phosphor Ba 2 SiO 4: Eu 2+, Ho 3+ and photostimulable luminescence for optical information storage. J Mater Chem C 2018;6:6058–67.

[49] An J, Zhao X, Li D, Zhang Y, Fei F, Pun E, et al. New insights into phosphorescence properties of LuAGG: long afterglow phosphor-in-glass for optical data storage. Ceram Int 2021;47:3185–94.

[50] Kang R, Nie J, Dou X, Zhang S, Ju G, Chen L, et al. Tunable NIR long persistent luminescence and discovery of trap-distribution-dependent excitation enhancement in transition metal doped weak-crystal-field CaZnGe2O6. J Alloys Compd 2018;735:692–9.

[51] Sun X, Zhang J, Zhang X, Luo Y, Wang X-J. Long lasting yellow phosphorescence and photostimulated luminescence in Sr3SiO5: Eu2+ and Sr3SiO5: Eu2+, Dy3+ phosphors. J Phys Appl Phys 2008;41:195414.

[52] Xiaoqin M, Lixin Y, Jiaju S, Songchu L, Zhong J. Synthesis and photoluminescent properties of Eu3+/Dy3+ doped SrO-Al2O3-SiO2 glass-ceramics. J Rare Earths 2017;35:446–52.

[53] Davis K. Material review: alumina (Al 2 O 3). School of Doctoral Studies European Union Journal 2010;1(1).

[54] Chen M, He F, Shi J, Xie J, Yang H, Wan P. Low Li2O content study in Li2O-Al2O3-SiO2 glass-ceramics. J Eur Ceram Soc 2019;39:4988–95.

[55] Kurajica S, Šipušić J, Zupancic M, Brautović I, Albrecht M. ZnO-Al2O3-SiO2 glass ceramics: influence of composition on crystal phases, crystallite size and appearance. J Non-Cryst Solids 2021;553:120481.

[56] Gao MC, Zhang B, Guo S, Qiao J, Hawk J. High-entropy alloys in hexagonal close-packed structure. Metall Mater Trans 2016;47:3322–32.

[57] Toya T, Tamura Y, Kameshima Y, Okada K. Preparation and properties of CaO–MgO–Al2O3–SiO2 glass-ceramics from kaolin clay refining waste (Kira) and dolomite. Ceram Int 2004;30:983–9.

[58] Savabieh H, Alizadeh P, Dasilva YAR, Erni R, Clemens FJ. Investigation of dielectric properties and microstructure of sintered 13· 2Li2O– 67· 6SiO2– 14.49 Al2O3– 3· 3TiO2– 0.4 BaO– 0.97 ZnO glass-ceramics. J Eur Ceram Soc 2017;37:631–9.

[59] Moo-Chin W, Nan-Chung W, Min-Hsiung H. Preparation of nepheline glass-ceramics and their application as dental porcelain. Mater Chem Phys 1994;37:370–5.

[60] Hamzawy EM, El-Meliegy EA. Preparation of nepheline glass–ceramics for dental applications. Mater Chem Phys 2008;112:432–5.

[61] Deshkar A, Ahmadzadeh M, Scrimshire A, Han E, Bingham PA, Guillen D, et al. Crystallization behavior of iron-and boron-containing nepheline (Na2O● Al2O3● 2SiO2) based glasses: implications on the chemical durability of high-level nuclear waste glasses. ALL RIGHTS RESERVED 2019:189.

[62] Mirdamadi ES, Nazarpak MH, Solati-Hashjin M. Metal oxide-based ceramics. In: Structural biomaterials. Elsevier; 2021. p. 301–31.

[63] Buerger M, Klein GE, Donnay G. Determination of the crystal structure of nepheline. Am Mineral: Journal of Earth and Planetary Materials 1954;39:805–18.

[64] Akinribide OJ, Mekgwe GN, Obadele BA, Ajibola OO, Akinwamide SO, Olubambi PA. Microstructural and phase evolution of spark plasma sintering of graphitized Ti (C0. 9N0. 1) composites. Int J Refract Metals Hard Mater 2019;78:164–9.

[65] Deshkar A, Ahmadzadeh M, Scrimshire A, Han E, Bingham PA, Guillen D, et al. Crystallization behavior of iron-and boron-containing nepheline (Na2O· Al2O3· 2SiO2) based model high-level nuclear waste glasses. J Am Ceram Soc 2019;102:1101–21.

[66] Kroll JO, Vienna JD, Schweiger MJ. Effects of Al2O3, B2O3, Li2O, Na2O, and SiO2 on nepheline crystallization in Hanford high level waste glasses. Advances in Materials Science for Environmental and Energy Technologies V: Ceram Trans 2016;260:159–69.

[67] Segets D, Gradl J, Taylor RK, Vassilev V, Peukert W. Analysis of optical absorbance spectra for the determination of ZnO nanoparticle size distribution, solubility, and surface energy. ACS Nano 2009;3:1703–10.

[68] Liu H, Yang D, Yang H, Zhang H, Zhang W, Fang Y, et al. Comparative study of respiratory tract immune toxicity induced by three sterilisation nanoparticles: silver, zinc oxide and titanium dioxide. J Hazard Mater 2013;248:478–86.

[69] Mirhosseini M, Firouzabadi FB. Antibacterial activity of zinc oxide nanoparticle suspensions on food-borne pathogens. Int J Dairy Technol 2013;66:291–5.

[70] Mason P. Physiological and medicinal zinc. Pharmaceut J 2006;276:271–4.

[71] Kołodziejczak-Radzimska A, Jesionowski T. Zinc oxide—from synthesis to application: a review. Materials 2014;7:2833–81.

[72] Newman MD, Stotland M, Ellis JI. The safety of nanosized particles in titanium dioxide–and zinc oxide–based sunscreens. J Am Acad Dermatol 2009;61:685–92.

[73] Kato K. Abrasive wear of metals. Tribol Int 1997;30:333–8.

[74] Roessler D, Walker W. Electronic spectrum and ultraviolet optical properties of crystalline MgO. Phys Rev 1967;159:733.

[75] Bishop A, Klein C, HurlbutJr CS. In: Manual of mineralogy (after james D. Dana) 1993. 58. John Wiley and Sons Inc.; 1994. p. 524–6. 681 pp.£ 22.95 plexicover,£ 62.00 cloth," Mineralogical Magazine.

[76] Choubey R, Sen P, Sen P, Bhatt R, Kar S, Shukla V, et al. Optical properties of MgO doped LiNbO3 single crystals. Opt Mater 2006;28:467–72.

[77] Itatani K, Tsujimoto T, Kishimoto A. Thermal and optical properties of transparent magnesium oxide ceramics fabricated by post hot-isostatic pressing. J Eur Ceram Soc 2006;26:639–45.

[78] Fang Y, Agrawal D, Skandan G, Jain M. Fabrication of translucent MgO ceramics using nanopowders. Mater Lett 2004;58:551–4.

[79] Li G, Edwards J, Carley AF, Hutchings GJ. Direct synthesis of hydrogen peroxide from H2 and O2 using zeolite-supported Au-Pd catalysts. Catal Today 2007;122:361–4.

[80] Kato T, Okada G, Yanagida T. Optical, scintillation and dosimeter properties of MgO transparent ceramic and single crystal. Ceram Int 2016;42:5617–22.

[81] Li C-J, Xu G-R, Zhang B, Gong JR. High selectivity in visible-light-driven partial photocatalytic oxidation of benzyl alcohol into benzaldehyde over single-crystalline rutile TiO2 nanorods. Appl Catal B Environ 2012;115:201–8.

[82] Zhao M, Sun Y, Zhang J, Zhang Y. Novel translucent and strong submicron alumina ceramics for dental restorations. J Dent Res 2018;97:289–95.

[83] Ding B, Zheng P, Ma Pa, Lin J. Manganese oxide nanomaterials: synthesis, properties, and theranostic applications. Adv Mater 2020;32:1905823.

[84] Na HB, Lee JH, An K, Park YI, Park M, Lee IS, et al. Development of a T1 contrast agent for magnetic resonance imaging using MnO nanoparticles. Angew Chem 2007;119:5493–7.

[85] Geng B, Liu X, Ma J, Du Q. A new nonhydrolytic single-precursor approach to surfactant-capped nanocrystals of transition metal sulfides. Mater Sci Eng, B 2007;145:17–22.

[86] Kruk A. Fabrication of MgO high transparent ceramics by arc plasma synthesis. Opt Mater 2018;84:360–6.

[87] Ray JC, Pati RK, Pramanik P. Chemical synthesis and structural characterization of nanocrystalline powders of pure zirconia and yttria stabilized zirconia (YSZ). J Eur Ceram Soc 2000;20:1289–95.

[88] Parker G. Encyclopedia of materials: science and technology. 2001.

[89] Elias CN, Duailibi Filho J, Oliveira LGd. Mechanical properties of alumina-zirconia composites for ceramic abutments. Mater Res 2004;7:643–9.

[90] Fan W, Bai Y, Wang Z, Che J, Wang Y, Tao W, et al. Effect of point defects on the thermal conductivity of Sc2O3-Y2O3 co-stabilized tetragonal ZrO2 ceramic materials. J Eur Ceram Soc 2019;39:2389–96.

[91] Zhang Y, Lawn B. Novel zirconia materials in dentistry. J Dent Res 2018;97:140–7.

[92] Wildgoose DG, Johnson A, Winstanley RB. Glass/ceramic/refractory techniques, their development and introduction into dentistry: a historical literature review. J Prosthet Dent 2004;91:136–43.

[93] Fu L, Jiang F, Li B, Cheng Y, Xu G, Huang J, et al. Doping of tantalum, niobium, and hafnium in a translucent ZrO2-SiO2 nanocrystalline glass-ceramic. J Eur Ceram Soc 2021;37(12). https://doi.org/10.1016/j.jeurceramsoc.2017.05.039.

[94] Akinribide OJ, Obadele BA, Ayeleru OO, Akinwamide S, Nomoto K, Eizadjou M, et al. The role of graphite addition on spark plasma sintered titanium nitride. J Mater Res Technol 2020;9:6268–77.

[95] Garvie RC, Hannink R, Pascoe R. Ceramic steel?. In: Sintering key papers. Springer; 1990. p. 253–7.

[96] Hannink RH, Kelly PM, Muddle BC. Transformation toughening in zirconia-containing ceramics. J Am Ceram Soc 2000;83:461–87.

[97] Fu L, Wang Y, Riekehr L, Räthel J, Engqvist H, Xia W. Observation of yttrium oxide segregation in a ZrO2-SiO2 glass-ceramic at nanometer dimensions. J Am Ceram Soc 2020;103:7147–58.

[98] Hou X, Zhang R, Fang D. An ultralight silica-modified ZrO2–SiO2 aerogel composite with ultra-low thermal conductivity and enhanced mechanical strength. Scripta Mater 2018;143:113–6.

[99] Gaboriaud R, Paumier F, Lacroix B. Disorder–order phase transformation in a fluorite-related oxide thin film: in-situ

X-ray diffraction and modelling of the residual stress effects. Thin Solid Films 2016;601:84–8.

[100] Li J, Wu Y, Pan Y, Liu W, Zhu Y, Guo J. Agglomeration of α-Al2O3 powders prepared by gel combustion. Ceram Int 2008;34:1539–42.

[101] Takahashi S, Kan A, Ogawa H. Microwave dielectric properties and crystal structures of spinel-structured MgAl2O4 ceramics synthesized by a molten-salt method. J Eur Ceram Soc 2017;37:1001–6.

[102] Ikegami T, Li JG, Mori T, Moriyoshi Y. Fabrication of transparent yttria ceramics by the low-temperature synthesis of yttrium hydroxide. J Am Ceram Soc 2002;85:1725–9.

[103] Serivalsatit K, Ballato J. Submicrometer grain-sized transparent erbium-doped scandia ceramics. J Am Ceram Soc 2010;93:3657–62.

[104] Saito N, Matsuda Si, Ikegami T. Fabrication of transparent yttria ceramics at low temperature using carbonate-derived powder. J Am Ceram Soc 1998;81:2023–8.

[105] Huang Y, Jiang D, Zhang J, Lin Q. Fabrication of transparent lanthanum-doped yttria ceramics by combination of two-step sintering and vacuum sintering. J Am Ceram Soc 2009;92:2883–7.

[106] Jin L, Zhou G, Shimai S, Zhang J, Wang S. ZrO_2-doped Y_2O_3 transparent ceramics via slip casting and vacuum sintering. J Eur Ceram Soc 2010;30:2139–43.

[107] Hou X, Zhou S, Jia T, Lin H, Teng H. Effect of Nd concentration on structural and optical properties of Nd: Y2O3 transparent ceramic. J Lumin 2011;131:1953–8.

[108] Eilers H. Fabrication, optical transmittance, and hardness of IR-transparent ceramics made from nanophase yttria. J Eur Ceram Soc 2007;27:4711–7.

[109] Badwal SP, Ciacchi FT, Giampietro KM. Analysis of the conductivity of commercial easy sintering grade 3 mol% Y_2O_3–ZrO_2 materials. Solid State Ionics 2005;176:169–78.

[110] Li JG, Ikegami T, Mori T. Fabrication of transparent, sintered Sc_2O_3 ceramics. J Am Ceram Soc 2005;88:817–21.

[111] Chen Q, Shi Y, An L, Chen J, Shi J. Fabrication and photoluminescence characteristics of Eu3+-doped Lu2O3 transparent ceramics. J Am Ceram Soc 2006;89:2038–42.

[112] Boulesteix R, Epherre R, Noyau S, Vandenhende M, Maitre A, Sallé C, et al. Highly transparent Nd: Lu2O3 ceramics obtained by coupling slip-casting and spark plasma sintering. Scripta Mater 2014;75:54–7.

[113] Akinribide OJ, Obadele BA, Akinwamide SO, Ayeleru OO, Eizadjou M, Ringer SP, et al. Microstructural characterization and mechanical behaviours of TiN-graphite composites fabricated by spark plasma sintering. Int J Refract Metals Hard Mater 2020:105253.

[114] Jiang L, Liao Y, Wan Q, Li W. Effects of sintering temperature and particle size on the translucency of zirconium dioxide dental ceramic. J Mater Sci Mater Med 2011;22:2429–35.

[115] Lee SH, Kochawattana S, Messing GL, Dumm JQ, Quarles G, Castillo V. Solid-state reactive sintering of transparent polycrystalline Nd: YAG ceramics. J Am Ceram Soc 2006;89:1945–50.

[116] Fan B, Li W, Zhang F, Li H, Zhang R, Liu G, et al. Fabrication and properties of Si2N2O ceramics for microwave sintering furnace. Processing and Application of Ceramics 2020;14:32–9.

[117] Chaim R. Densification mechanisms in spark plasma sintering of nanocrystalline ceramics. Mater Sci Eng, A 2007;443:25–32.

[118] Drdlíková K, Klement R, Drdlík D, Spusta T, Galusek D, Maca K. Luminescent Er3+ doped transparent alumina ceramics. J Eur Ceram Soc 2017;37:2695–703.

[119] Nanko M, Dang K. Two-step pulsed electric current sintering of transparent Al2O3 ceramics. Adv Appl Ceram 2014;113:80–4.

[120] Mata-Osoro G, Moya JS, Pecharroman C. Transparent alumina by vacuum sintering. J Eur Ceram Soc 2012;32:2925–33.

[121] Stuer M, Zhao Z, Aschauer U, Bowen P. Transparent polycrystalline alumina using spark plasma sintering: effect of Mg, Y and La doping. J Eur Ceram Soc 2010;30:1335–43.

[122] Roussel N, Lallemant L, Durand B, Guillemet S, Ching J-YC, Fantozzi G, et al. Effects of the nature of the doping salt and of the thermal pre-treatment and sintering temperature on Spark Plasma Sintering of transparent alumina. Ceram Int 2011;37:3565–73.

[123] Suárez M, Fernández-Camacho A, Torrecillas R, Menéndez JL. Sintering to transparency of polycrystalline ceramic materials. InTech; 2012.

[124] Schehl M, Dıaz L, Torrecillas R. Alumina nanocomposites from powder–alkoxide mixtures. Acta Mater 2002;50:1125–39.

[125] Chang Y-C, Lee W-J, Yang H-H, Wang L-C, Lu J-H, Tsai YI, et al. Reducing emissions of persistent organic pollutants from a diesel engine by fueling with water-containing butanol diesel blends. Environ Sci Technol 2014;48:6010–8.

[126] Yang K-C, Shen P, Gan D. On the reorientation of ZrTiO4 particles during reactive sintering of TiO2–ZrO2. J Eur Ceram Soc 2008;28:1169–76.

[127] Zhou Z, Li W, Song J, Yi G, Mei B, Su L. Synthesis and characterization of Nd3+ doped SrF2 nanoparticles prepared by precipitation method. Ceram Int 2018;44:4344–50.

[128] Liu X, Chu PK, Ding C. Surface modification of titanium, titanium alloys, and related materials for biomedical applications. Mater Sci Eng R Rep 2004;47:49–121.

[129] Li T, Wang J, Ruan J, Liu C, Han J. Crystallization behavior of transparent Na2O-Al2O3-SiO2 glass-ceramic containing rare-earth oxides. J Non-Cryst Solids 2021;567:120935.

[130] Haertling GH, Land CE. Hot-pressed (Pb, La)(Zr, Ti) O3 ferroelectric ceramics for electrooptic applications. J Am Ceram Soc 1971;54:1–11.

[131] Gibson PW, Lee C, Ko F, Reneker D. Application of nanofiber technology to nonwoven thermal insulation. Journal of Engineered Fibers and Fabrics 2007;2:155892500700200204.

[132] Bi Y, Zhang H, Wang H, Jia Q, Zhang S. Facile preparation of reduced GO modified porous ceramics with hierarchical pore structure as a highly efficient and durable sorbent material. J Eur Ceram Soc 2020;40:2106–12.

[133] She J, Ohji T. Fabrication and characterization of highly porous mullite ceramics. Mater Chem Phys 2003;80:610–4.

[134] Miao X. Porous mullite ceramics from natural topaz. Mater Lett 1999;38:167–72.

[135] Dong Y, Diwu J, Feng X, Feng X, Liu X, Meng G. Phase evolution and sintering characteristics of porous mullite ceramics produced from the flyash-Al (OH) 3 coating powders. J Alloys Compd 2008;460:651–7.

[136] Qian H, Cheng X, Zhang H, Zhang R, Wang Y. Preparation of porous mullite ceramics using fly ash cenospheres as a pore-forming agent by gelcasting process. Int J Appl Ceram Technol 2014;11:858–63.

[137] Bai J. Fabrication and properties of porous mullite ceramics from calcined carbonaceous kaolin and α-Al2O3. Ceram Int 2010;36:673–8.

[138] Yang M, Luo X, Yi J, Yu M, Zhang X. A novel way to fabricate fibrous mullite ceramic using sol-gel vacuum impregnation. Ceram Int 2018;44:12664–9.

[139] Han L, Deng X, Li F, Huang L, Pei Y, Dong L, et al. Preparation of high strength porous mullite ceramics via combined foam-gelcasting and microwave heating. Ceram Int 2018;44:14728–33.

[140] Liu Y-F, Liu X-Q, Wei H, Meng G-Y. Porous mullite ceramics from national clay produced by gelcasting. Ceram Int 2001;27:1–7.

[141] Yuan L, Liu Z, Yan Z, Jin E, Tian C, Yu J. Effect of mullite phase formed in situ on pore structure and properties of high-purity mullite fibrous ceramics. Ceram Int 2021;27(1):1–7. https://doi.org/10.1016/S0272-8842(00)00034-1.

[142] Pomeroy M. Encyclopedia of materials: technical ceramics and glasses. Elsevier; 2021.

[143] Patterson MC, DiGiovanni AA, Fehrenbacher L, Roy DW. Spinel: gaining momentum in optical applications. In: Window and dome technologies Viii; 2003. p. 71–9.

[144] Goldman LM, Hartnett TM, Wahl JM, Ondercin RJ, Olson KR. Recent advances in aluminum oxynitride (ALON) optical ceramic. Window and dome technologies and materials Vii 2001;4375:71–8.

[145] de Groot JJ, Van Vliet J. The high-pressure sodium lamp. Macmillan International Higher Education; 1986.

[146] Seinen P. High intensity discharge lamps with ceramic envelopes. Proc. of 7th Int. Sympo. Sci. & Tech. Light Sources 1995:101–9.

[147] Juengst S, Lang D, Galvez M. Arc tubes for improved isothermal operation. Proc. 10th int. sym. sci. & tech. of light sources 2004:115–24.

[148] Krell A, Hutzler T, Klimke J. Transparent ceramics for structural applications: part 2: fields of applications. In: CFI. Ceramic forum international; 2007.

[149] Niimi N. Translucent ceramic, a method of producing the same and discharge vessels. Google Patents; 2005.

[150] Stoimenov PK, Klinger RL, Marchin GL, Klabunde KJ. Metal oxide nanoparticles as bactericidal agents. Langmuir 2002;18:6679–86.

[151] Hříbalová S, Pabst W. Modeling light scattering by spherical pores for calculating the transmittance of transparent ceramics–All you need to know. J Eur Ceram Soc 2021;41:2169–92.

[152] Krell A, Hutzler T, Klimke J. Transmission physics and consequences for materials selection, manufacturing, and applications. J Eur Ceram Soc 2009;29:207–21.

[153] Apetz R, Van Bruggen MP. Transparent alumina: a light-scattering model. J Am Ceram Soc 2003;86:480–6.

[154] Wang Y, Zhang R, He J, Tian M, Zhang T, Shang P, et al. Light scattering by composition inhomogeneity and residual pores in LiAlON solid solution transparent ceramics. Ceram Int 2019;45:21029–33.

[155] Wang J, Shaw LL. Transparent nanocrystalline hydroxyapatite by pressure-assisted sintering. Scripta Mater 2010;63:593–6.

[156] Bodhak S, Balla VK, Bose S, Bandyopadhyay A, Kashalikar U, Jha SK, et al. In vitro biological and tribological properties of transparent magnesium aluminate (Spinel) and aluminum oxynitride (ALON®). J Mater Sci Mater Med 2011;22:1511–9.

[157] Krishnan M, Tiwari B, Seema S, Kalra N, Biswas P, Rajeswari K, et al. Transparent magnesium aluminate spinel: a prospective biomaterial for esthetic orthodontic brackets. J Mater Sci Mater Med 2014;25:2591–9.

[158] Williams DF. On the mechanisms of biocompatibility. Biomaterials 2008;29:2941–53.

Dr. O.J. Akinribide is a Principal Engineer in the Research and Development Department, Engineering Materials Development Institute, Akure, and a Postdoctoral Research Fellow lecturer in the Department of Metallurgical Engineering, University of Johannesburg, South Africa. He is a renowned Materials Engineer and a registered engineer with the Council for Regulation of Engineering in Nigeria (COREN). Currently a Professional Member of the Institute of Materials, Minerals, and Mining (IOM3) with Professional Membership (MIMMM), United Kingdom. Moreover, he is currently serving as a reviewer of six scientific journals including the Vacuum; Elsevier, Current Journal of Applied Science and Technology, Journal of Materials Science (Springer nature), Journal of Process Mechanical Engineering (SAGE), Particulate Science and Technology (Taylor and Francis) and Materials Today: Proceedings among others).

Professor P.A Olubambi's current research activities are focused on three key and interrelated fields of advanced materials; “Powder Metallurgy”, “Nanomechanics” and “Tribocorrosion”. He centers his research efforts on the utilization of innovative powder metallurgical techniques for developing high strength, high temperature, and tribocorrosion resistance metallic alloys and metal-ceramics composites for the extreme environments in the aerospace, mines, chemical, and allied industries as well as for biomedical applications. He is currently the Head of the Centre for Nanomechanics and Tribocorrosion, and the Head of the School of Mining, Metallurgy and Chemical Engineering, University of Johannesburg, South Africa.

Dr. S.O. Akinwamide is a Postdoctoral Research Fellow in the Department of Mechanical Engineering, Aalto University, and Espoo, Finland. He is a renowned researcher in the field of Materials Engineering and is currently a Professional Member of the Institute of Materials, Minerals, and Mining with Professional Membership (MIMMM), United Kingdom.

Ms. G.N Mekgwe is currently a Ph.D. student of Metallurgical Engineering at the center for Nanomechanics and Tribocorrosion (CNT), University of Johannesburg, South Africa. She is a renowned researcher in Composite Engineering.

Professor Fehmi Gamaoun is a senior lecturer and associate at King Khalid University, Saudi Arabia. He is currently a winner of deanship scientific research at the Mechanical Engineering Department, College of Engineering, King Khalid University, Abha, Saudi Arabia, He has successfully supervised several Doctoral and Masters Students. His research interests include Shape Memory Alloys, Smart Materials, Mechanical Properties, Microstructure, Materials, Material Characterization Mechanical Behavior of

Materials, Advanced Materials, Mechanical Testing, Mechanics of Materials, Tensile tests, Fracture Mechanics, Experimental Mechanics, Plasticity, Material Characteristics, Metallurgical Engineering, Materials Testing, Tensile Testing, Recrystallization, SEM Analysis Corrosion Materials Technology, Surface Engineering, Nanoindentation, Dislocation Mechanics among others.

Dr Chamil received the B.Sc. (Hons.) degree in mechanical engineering from the University of Peradeniya, Sri Lanka, in 2007, with the award of best performance in mechanical engineering, and the Ph.D. degree in mechanical engineering from the Queens University Belfast, U.K., in 2011, with several publications, in which one of his publications received the Young Author Best Paper Award from the IEEE in 2011. After completing the Ph.D. degree, he briefly worked as a Lecturer in Mechanical Engineering with the University of Peradeniya, Sri Lanka, a Research Fellow with the University of Bradford, U.K., and a Lecturer of Engineering with the Glyndwr University, U.K., before joining the UoM. Currently, Chamil is a Senior Lecturer and working mainly with the Northwest Composts Centre and the Aerospace Research Institute, and supervising research students affiliated with the School of Materials, UoM, and the School of Mechanical and Aerospace Engineering, UoM. So far, he has authored 60+ peer-reviewed journals/conference papers. Moreover, he has authored a monograph, “Polymer Extrusion: A Study on Thermal Monitoring Techniques and Melting Issues.” His current research interests include: process monitoring, modeling, and control; soft sensors and soft sensing; process instrumentation; renewable energy technologies; 3D printing, phase change materials; and heat transfer. Chamil's current research activities are funded by several local and international companies and also by the professional funding bodies. He is a Charted Engineer and also an Associate Member of the professional bodies, including IESL, IMechE, IOM3 and ICPM; and also a Fellow of the Higher Education Academy, U.K. Moreover, he is currently serving as an Associate Editor of seven scientific journals including the Journal of Fluid Flow, Heat and Mass Transfer and Composites Communications. Furthermore, he has been served on scientific committees, and has also been invited for keynote speeches of several international conferences.